European Journal of Cell Biology 103 (2024) 151406

Contents lists available at ScienceDirect

European Journal of Cell Biology

journal homepage: www.elsevier.com/locate/ejcb

The solute carrier SLC7A1 may act as a protein transporter at the blood-brain barrier

Magdalena Kurtyka [a], Frank Wessely [b], Sarah Bau [c], Eseoghene Ifie [d], Liqun He [e], Nienke M. de Wit [f,g], Alberte Bay Villekjær Pedersen [h], Maximilian Keller [a], Caleb Webber [b], Helga E. de Vries [f,g], Olaf Ansorge [d], Christer Betsholtz [e,i], Marijke De Bock [j], Catarina Chaves [k], Birger Brodin [h], Morten S. Nielsen [l], Winfried Neuhaus [m,n], Robert D. Bell [o], Tamás Letoha [p], Axel H. Meyer [q], Germán Leparc [r], Martin Lenter [s], Dominique Lesuisse [k], Zameel M. Cader [d], Stephen T. Buckley [t], Irena Loryan [u], Claus U. Pietrzik [a,*]

[a] Institute for Pathobiochemistry, University Medical Center Mainz, Mainz, Germany
[b] UK Dementia Research Institute, Cardiff University, Cardiff, United Kingdom
[c] Pathology & Imaging, Novo Nordisk A/S, Måløv, Denmark
[d] Nuffield Department of Clinical Neurosciences, University of Oxford, Oxford, United Kingdom
[e] Department of Immunology, Genetics and Pathology, Rudbeck Laboratory, Uppsala University, Uppsala, Sweden
[f] Amsterdam UMC location Vrije Universiteit Amsterdam, Department of Molecular Cell Biology and Immunology, Amsterdam, the Netherlands
[g] Amsterdam Neuroscience, Amsterdam, the Netherlands
[h] Department of Pharmacy, University of Copenhagen, Copenhagen, Denmark
[i] Department of Medicine (Huddinge), Karolinska Institutet, Huddinge, Sweden
[j] Neuroscience Discovery, Janssen Research & Development, Janssen Pharmaceutica, Beerse, Belgium
[k] Rare and Neurologic Diseases Research Therapeutic Area, Sanofi, Chilly Mazarin, France
[l] Department of Biomedicine, Faculty of Health, Aarhus University, Aarhus, Denmark
[m] Austrian Institute of Technology GmbH, Vienna, Austria
[n] Department of Medicine, Faculty of Medicine and Dentistry, Danube Private University, Krems, Austria
[o] Ascidian Therapeutics Inc., Boston, USA
[p] Pharmacoidea Ltd., Szeged, Hungary
[q] AbbVie Deutschland GmbH & Co. KG, Quantitative, Translational & ADME Sciences, Ludwigshafen, Germany
[r] Boehringer Ingelheim Pharma GmbH & Co. KG, Translational Medicine & Clinical Pharmacology, Biberach, Germany
[s] Boehringer Ingelheim Pharma GmbH & Co. KG, Drug Discovery Sciences, Biberach, Germany
[t] Global Research Technologies, Novo Nordisk A/S, Måløv, Denmark
[u] Department of Pharmacy, Uppsala University, Uppsala, Sweden

ARTICLE INFO

Keywords:
BBB
brain drug delivery
brain therapeutics
CAT-1

ABSTRACT

Despite extensive research, targeted delivery of substances to the brain still poses a great challenge due to the selectivity of the blood-brain barrier (BBB). Most molecules require either carrier- or receptor-mediated transport systems to reach the central nervous system (CNS). These transport systems form attractive routes for the delivery of therapeutics into the CNS, yet the number of known brain endothelium-enriched receptors allowing the transport of large molecules into the brain is scarce. Therefore, to identify novel BBB targets, we combined

Abbreviations: AD, Alzheimer's disease; BBB, blood-brain barrier; BBB-TT, blood-brain barrier transport targets; bEnd.3, mouse brain endothelioma cells; (H/M) BMEC, (human/murine) brain microvascular endothelial cells; BSA, bovine serum albumin; CHO, Chinese hamster ovary; CNS, central nervous system; HCMEC/D3, immortalised human brain capillary endothelial cells; HHSEC, human hepatic sinusoidal endothelial cells; INSR, insulin receptor; ISH, in situ hybridization; HCT, human colorectal carcinoma; HEK, human embryonic kidney; KO, knock-out; MEF, mouse embryonic fibroblasts; NO-, nitric oxide; OE, over-expression; PECAM1, Platelet endothelial cell adhesion molecule 1; PNGase F, Peptide:N-glycosidase F; HPMEC, human pulmonary microvascular endothelial cells; RMT, receptor-mediated transport; RNA-seq, RNA sequencing; RT, room temperature; SLC, solute carrier; SLC7A1/CAT-1, high-affinity cationic amino acid transporter 1; SWOT, Strengths, Weaknesses, Opportunities, Threats; TBS, Tris-buffered saline; TBST;, Tris-buffered saline with Tween 20; TBSTx, Tris-buffered saline with Triton X-100; TCA, trichloroacetic acid; TEER, transendothelial electric resistance; TF, transferrin; TFRC, transferrin receptor; TQ, transcytosis quotient; WT, wild-type; ZO-1, zona occludens-1.

* Corresponding author.
E-mail address: pietrzik@uni-mainz.de (C.U. Pietrzik).

https://doi.org/10.1016/j.ejcb.2024.151406
Received 1 December 2023; Received in revised form 2 March 2024; Accepted 20 March 2024
Available online 21 March 2024

SLC7A1
solute carriers

transcriptomic analysis of human and murine brain endothelium and performed a complex screening of BBB-enriched genes according to established selection criteria. As a result, we propose the high-affinity cationic amino acid transporter 1 (SLC7A1) as a novel candidate for transport of large molecules across the BBB. Using RNA sequencing and in situ hybridization assays, we demonstrated elevated *SLC7A1* gene expression in both human and mouse brain endothelium. Moreover, we confirmed SLC7A1 protein expression in brain vasculature of both young and aged mice. To assess the potential of SLC7A1 as a transporter for larger proteins, we performed internalization and transcytosis studies using a radiolabelled or fluorophore-labelled anti-SLC7A1 antibody. Our results showed that SLC7A1 internalised a SLC7A1-specific antibody in human colorectal carcinoma (HCT116) cells. Moreover, transcytosis studies in both immortalised human brain endothelial (hCMEC/D3) cells and primary mouse brain endothelial cells clearly demonstrated that SLC7A1 effectively transported the SLC7A1-specific antibody from luminal to abluminal side. Therefore, here in this study, we present for the first time the SLC7A1 as a novel candidate for transport of larger molecules across the BBB.

1. Introduction

Central nervous system (CNS) disorders became one of the biggest burdens for public health worldwide. World Health Organization ranked stroke, Alzheimer's disease (AD) and other dementias in the top seven global causes of death in 2019, whereas neurological disorders were the primary cause of disability already in 2016 (Feigin et al., 2019; World Health Organization, 2020). In 2004, the first monoclonal antibodies (mAbs) have been approved by the FDA for the treatment of neurological diseases such as chronic migraine and multiple sclerosis (Gklinos et al., 2021). Despite the undoubted success of these therapies, the majority of CNS pathologies lack effective treatment. This is partly due to the fact that current therapeutic mAbs do not effectively cross the blood-brain barrier (BBB) but act peripherally. Inefficient transport of therapeutics across the BBB is the major obstacle to the successful treatment of CNS disorders, including neurodegenerative diseases.

The BBB consists of tightly connected endothelial cells lining the brain capillaries, surrounded by pericytes and astrocytes (Abbott et al., 2010; Keaney and Campbell, 2015; Profaci et al., 2020). Brain microvascular endothelial cells (BMEC) lack fenestrae and show an extremely low rate of transcytosis (Ben-Zvi et al., 2014). Moreover, BMEC form a polarized interface between brain parenchyma and blood compartments thanks to tight and adherent junction complexes and differential composition of lipids and membrane proteins at luminal and abluminal membrane (Worzfeld and Schwaninger, 2016). Due to these unique features of the BBB, only small, lipid-soluble, non-polar molecules, which are not efflux transporters substrates, can freely diffuse into the brain parenchyma (Banks, 2016; Kadry et al., 2020). While junction complexes prevent the paracellular diffusion of soluble substances across the BBB, the majority of large molecules require specific transporters or receptors (O'Keeffe and Campbell, 2016). Approaches for drug delivery across the BBB focus on either modifying ligands for already investigated transporters to improve the drug uptake, or discovering new targets for therapeutics delivery into the CNS. Many receptors responsible for the receptor-mediated transport (RMT) of large molecules, such as transferrin receptor (TFRC) (Johnsen et al., 2019; Kariolis et al., 2020; Okuyama et al., 2019), lipoprotein receptors (Kumthekar et al., 2020; Sakamoto et al., 2017; Storck et al., 2016) or insulin receptor (INSR) (Boado and Pardridge, 2017) have been intensively tested for their ability to deliver therapeutics into the CNS in preclinical and clinical studies. In fact, there is a very limited number of FDA-approved drugs for the treatment of CNS disorders (Pardridge, 2022), and only one RMT- targeting drug, Izcargo®, has been recently approved for clinical use in Japan (Okuyama et al., 2021; Yamamoro and Kawashima, 2022).

The aim of our study was to identify and validate novel candidate transporters for the delivery of large molecules, e.g., mAbs to the brain. First, we combined existing transcriptomic data on mouse endothelium (Vanlandewijck et al., 2018) with transcriptomic data generated from bulk RNA-sequencing (RNA-seq) of human brain endothelium (Leberer and Mastrobattista, 2022), to identify enriched genes. Next, we performed single-nucleus RNA-seq of human brain microvessels to narrow down the list of BBB-enriched genes. Furthermore, we established a three-step prioritization panel to screen the most promising novel BBB transport targets (BBB-TT). As a result of the joint transcriptomic and criteria-based screening, we selected SLC7A1 alias CAT-1 (high-affinity cationic amino acid transporter 1) as a novel potential target for drug delivery to the brain. Using a broad panel of techniques, we evaluated SLC7A1 gene and protein expression in both mouse and human brain endothelium. Finally, we explored SLC7A1 potential as a functional transporter of larger molecules in transport studies using radiolabelled or fluorophore-labelled specific anti-SLC7A1 antibody in SLC7A1 knock-out cells, human brain endothelial hCMEC/D3 cells as well as primary murine brain endothelial cells.

2. Materials and methods

All chemicals and reagents were purchased from Merck (Darmstadt, Germany) unless otherwise stated.

2.1. Mice tissue

The 3-months- and 2-year-old wild-type (WT) C57Bl/6 J male mice were deeply anesthetized by isoflurane inhalation before transcardially perfused with 0.9% saline, followed by 10% neutral-buffered formalin fixation (flow rate: 5 mL/min). Fixed samples were then dehydrated in a series of increasing ethanol concentrations followed by xylene clearing on the tissue processor (Leica ASP300S, Mannheim, Germany) and embedding in paraffin.

2.2. Human tissue

For bulk RNA sequencing (RNA-seq), human brain microvascular endothelial cells (HBMEC), human pulmonary microvascular endothelial cells (HPMEC) and human hepatic sinusoidal endothelial cells (HHSEC) were purchased from ScienCell™ Research Laboratories (Carlsbad, CA, USA) and Innoprot (Derio, Biskaia, Spain) (detailed overview: Suppl. Spreadsheet S1). Cells were grown in a fibronectin-coated T-75 flask at 37 °C with 5% CO_2 in Endothelial Cell Medium, supplemented with 10% fetal bovine serum and Endothelial Cell Growth Supplement (all from ScienCell™ Research laboratories, Carlsbad, CA, USA). Cells were harvested after two passages to achieve the sufficient quantity of material necessary for RNA-seq.

For ISH experiments, the post-mortem human brain tissue was provided by Edinburgh Brain & Tissue Bank (BBN_19690, BBN_20995, BBN001.35416, BN001.35159, BBN_18407, BBN_24781) and approved by the local Committees on Health Research Ethics (H17014257). All material has been collected from donors after written informed consent for brain autopsy and use of brain tissue and clinical information for research purposes.

2.3. Bulk RNA-seq library preparation

8 samples of HBMEC, 6 samples of HPMEC and 6 samples of HHSEC

were used for bulk RNA-seq. Total RNA was individually extracted using the Ambion MagMAXTM-96 total RNA isolation kit (ThermoFisher, Braunschweig, Germany) according to the manufacturer's instructions. RNA quality and concentration were measured using the Fragment Analyser (AATI). RNA samples showed consistently high RIN (RNA integrity number) values of at least 7.6 except for one HBMEC sample (RIN value of 2.4). Sequencing library preparation was done using 200 ng of total RNA input with the TruSeq RNA Sample Prep Kit Set B (RS-122–2102, Illumina Inc., San Diego, CA, USA) producing 275 bp fragments including adapters on average size. Prior to sequencing, 12 individual libraries were normalized and pooled together using the adapter indices supplied by the manufacturer. Pooled libraries were clustered on the cBot instrument using the HS 3000/4000 SR Cluster Kit - cBot - HS (GD-410–1001, Illumina Inc.). Sequencing was then performed as 52 bp single-end reads and 7 bases index read on an Illumina HiSeq 3000 instrument using the TruSeq SBS Kit HS-v3 (50-cycle) (FC-401–3002, Illumina Inc.). Illumina sequencing resulted in approximately 24 million reads on average per sample. RNA-seq data are available at Gene Expression Omnibus under accession number: GSE226607.

2.4. Bulk RNA-seq analysis

Salmon (v0.13.1) (Patro et al., 2017) was used to map raw sequencing reads to a human reference transcriptome combining cDNA plus ncRNA and for which alternative sequences were removed before mapping (Ensembl GRCh38 version 98). The Salmon index was generated with k-mer length -k 23 due to shorter read length. Default Salmon mapping options were applied including the additional option –validateMappings. Salmon quantification data were imported and summarised on the gene level using the tximeta R package (v1.4.5) (Love et al., 2020). Quality control showed that the single brain sample with very low RIN value had a very low mapping rate of 14.5% and was therefore excluded from downstream analysis. The average mapping rate of all other samples (19) was approximately 91%. Additionally, two lung samples were also removed as they were detected as outliers in the principal components analysis along the first principal component. Canonical endothelial gene markers (*PECAM1*, *VWF*, *CDH5*) were highly expressed in all samples confirming their endothelial identity being retained through passaging of cells (Suppl. Fig. S1A). Those genes fall within the top 2% of ranked protein-coding genes, based on expression levels in all individual samples, except for *PECAM1* and *CDH5* in two brain samples. Pairwise differential gene expression analysis was performed on 17 samples with DESeq2 (v1.26.0) (Love et al., 2014) using protein-coding genes and an adjusted p-value cut-off 0.05 and a minimum effect size of one (log2 fold change) to obtain genes up-regulated in brain microvascular endothelial cells compared to the two other tissues. Human to mouse 1:1 orthologs were identified with the biomaRt R package (v2.42.1, sep2019 Ensembl archive).

2.5. Mouse transcriptomic data

To identify mouse brain microvascular endothelial cells (MBMEC) specific genes, we used previously published mouse brain and lung single-cell dataset (He et al., 2018). In this study, 405 MBMEC and 475 mouse pulmonary microvascular endothelial cells (MPMEC) were reported. The two cell populations were compared using the FindMarkers function of the Seurat R package (v3.1.1). The default Wilcoxon Rank Sum test was used to compare the two endothelial cells groups. Genes expressed in at least 25% of MBMEC, with minimum log2 fold change of 1 and with multiple test corrected p-value < 0.05 were identified as significantly up-regulated in MBMEC to MPMEC (Suppl. Spreadsheet S2). Using the same method, MBMEC were also compared to all other brain cell types identified in this mouse brain atlas, and genes up-regulated in MBMEC were identified (Suppl. Spreadsheet S3).

2.6. Vascular nuclei isolation from frozen post-mortem brain tissue

Human brain tissue was retrieved 3 days post-mortem by the Oxford Brain Bank (REC reference 15/SC/0639) and sectioned into two hemispheres. One hemisphere was fixed in 10% neutral-buffered formaldehyde, the other sliced in the coronal plane, flash frozen in liquid nitrogen and stored at −80 °C. Cases utilized included healthy control brain tissue and Braak stage 6 AD confirmed by immunostaining against amyloid beta (Suppl. Fig. S1B) (Braak and Braak, 1991). All procedure was carried out on ice and all equipment were pre-chilled to 4 °C before usage. Briefly, 1 g of frontal cortex brain tissue was thawed in 1 mL of ice-cold lysis buffer (8 g/L NaCl, 400 mg/L KCl, 185.4 mg/L $CaCl_2$.2 H_20, 60 mg/L KH_2PO4, 200 mg/L MgSO4•7 H_2O, 350 mg/L $NaHCO_3$, 1 g/L dextrose anhydrous, 90 mg/L Na_2HPO_4•7 H_2O, pH 7.4). Devoid of meninges tissue was then minced and homogenized with a motorized pestle mixer. The homogenate was centrifuged at 2000 *g* for 10 min and the resulting pellet containing vascular fraction was resuspended in chilled 16% dextran (70,000 Da) solution and centrifuged at 10,000 *g* for 15 min. Supernatant was removed and pellets were resuspended in 10 mL lysis buffer containing 5 mg/mL bovine serum albumin (BSA). The vascular fraction was then filtered through 300 μm and 40 μm strainers to retain the large vessels and microvessels, respectively. Microvessels were pelleted at 500 *g* for 5 min, fixed in paraformaldehyde (PFA) and immunostained using anti-CD31 endothelium marker. For nuclei isolation, endothelial cells were lysed for 20 min in nuclei lysis buffer (10 mM Tris-HCL, 10 mM NaCl, 3 mM $MgCl_2$, 25 mM KCl, 320 mM sucrose, 1 μM DTT, 0.01% digitonin, 0.30% NP40, 0.2 U/μL RNAse inhibitor) and homogenized using Dounce homogenizer (100 strokes). This step was repeated three times and nuclei isolation process was monitored using trypan blue staining. For purification purpose, 500 μL nuclei washing buffer (1x phosphate buffered saline (PBS); 1x BSA; 0.2 U/μL RNAse inhibitor) was added and nuclei were centrifuged at 500 *g* for 5 min. Nuclei were then filtered through 30 μm strainer, pelleted at 500 *g* for 5 min. Small fraction of enriched nuclei was stained with DAPI (1:1000) for validation purposes and the remaining sample was sorted on the SH800 Sony Cell Sorter (20,000 nuclei per sample) (Sony Biotechnology, San Jose, CA, USA) (Suppl. Fig. S1C).

2.7. 10X single-nuclei RNA-seq library preparation

The Chromium Single Cell 3pr single cell RNAseq version 3 reagent kit (10x Genomics, Pleasanton, CA, USA) was used. Nuclei were loaded onto each channel of the Chromium Chip G following manufacturer's instructions and the chip was inserted in the Chromium Controller for droplet encapsulation. Following GEM generation and barcoding, cDNA amplification was performed for 12 cycles, and gene expression library construction using 14 cycles of sample index PCR was performed according to manufacturer's protocol (CG000204). Single nuclei gene expression libraries were then sequenced on the Illumina NovaSeq 6000 system (Illumina Inc.) at a targeted depth of at least 50,000 reads per nucleus, using the following parameters: Read1: 28 bp i7: 8 bp, Read2: 98 bp cycles.

2.8. Single-nuclei RNA-seq analysis

CellRanger (v4.0.0, 10X Genomics) was used to map sequencing reads to the reference genome (refdata-gex-GRCh38–2020-A), which was modified as a pre-mRNA reference to also count intronic reads. CellRanger called approximately 2100 nuclei for each sample. The filtered feature-barcode matrices were used as input to downstream processing by the Seurat R package (v4.2.1) (Satija et al., 2015). Seurat processing included standard filtering of low-quality nuclei excluding nuclei with fewer than 200 features, more than 5000 features or more than 5% mitochondrial counts. Genes were excluded if not found as expressed in at least 3 nuclei. Default Seurat settings were used for downstream analysis. The first 30 principal components were used for a

dimensionally reduced representation of the data and the resolution parameter to obtain clusters was set to 0.4. Clusters were annotated to cell types based on typical cell type marker genes previously published (Grubman et al., 2019; Mathys et al., 2019) found as up-regulated in respective clusters by applying Seurat's function FindAllMarkers(min.pct = 0.25).

2.9. In situ hybridization assay

4.5 μm sections of the human formalin-fixed paraffin-embedded tissue blocks were sectioned using a microtome and applied to Superfrost Plus glass slides (ThermoFisher, Braunschweig, Germany). ISH was performed using the automated Ventana Discovery Ultra System equipped with the RNAscope Duplex Reagent kit (Roche, Mannheim, Germany) as described previously (Pyke, 2020). All the probes used were obtained from Advanced Cell Diagnostics (Newark, CA, USA) (Suppl. Spreadsheet S4). Brightfield images were acquired with the VS200 digital slide scanner (Olympus, Tokyo, Japan) using a UPLXAPO 40x/0.95 air objective.

2.10. Isolation and culture of mouse brain endothelial cells

MBMEC were isolated from 2-month-old WT mice and cultured in collagen IV/ fibronectin-coated 24-well Transwell filters (0.4 μm pore size; transparent, Sarstedt, Nümbrecht, Germany) as described previously (Pflanzner et al., 2011). Measurements of transendothelial electric resistance (TEER) and capacitance were conducted throughout the culture period using the cellZscope® system (nanoAnalytics, Münster, Germany). TEER values above 50 Ω•cm^2 and capacitance values below 1 μF/cm^2 were considered indicators of the confluent monolayer formation (Ruck et al., 2014; Weidenfeller et al., 2005). Sixteen hours before transport studies, culture medium was replaced with serum-free DMEM/Ham's F12 (Gibco, Darmstadt, Germany) (1:1 vol/vol ratio) supplemented with 1% penicillin/streptomycin and 550 nM hydrocortisone to boost tight junctions formation and increase TEER values (Hoheisel et al., 1998).

2.11. Isolation of murine cerebral microvessels

Microvessels were isolated based on dextran gradient centrifugation method followed by cell-strainer filtration described elsewhere with some modifications (Bell et al., 2012; Lee et al., 2019). Briefly, devoid of meninges cortices were fragmentated in ice-cold homogenization buffer (DPBS; 2.5 mM $CaCl_2$; 1.2 mM $MgSO_4$; 15 mM HEPES; 25 mM $NaHCO_3$; 10 mM glucose; 1 mM sodium pyruvate) using Dounce tissue grinder (10 strokes) and centrifuged at 1000 *g* for 10 min at 4 °C. The resulting pellet was resuspended in 18% Dextran (70,000 Da) solution in PBS and centrifuged at 4000 *g* for 20 min at 4 °C. Red capillary pellet at the bottom of the tubes was collected and filtered through a 40-μm cell nylon-mesh strainer (pluriSelect, Leipzig, Germany). Mesh was rinsed with ice-cold PBS and microvessels remaining on the top of the mesh were collected in 0.5% BSA/PBS solution. Samples were centrifuged at 4000 *g* for 12 min at 4 °C and resulting pellets were then lysed with microvessels lysis buffer (50 mM HEPES, pH 7.5; 1% (v/v) Triton X-100; 0.5% (w/v) sodium deoxycholate; 0.1% (w/v) SDS; 500 mM NaCl; 10 mM $MgCl_2$; 50 mM β-glycerophosphate; 1x cOmplete™ protease inhibitor cocktail; 1x PhosStop™ phosphatase inhibitor cocktail (both inhibitors from Roche, Mannheim, Germany).

2.12. Western blot

Cells were lysed in NP40 lysis buffer (50 mM Tris pH 8, 150 mM NaCl, 0.02% [w/v] NaN_3, 1% [v/v] Nonidet P-40; phosphatase and proteinase inhibitors (PhosSTOP™, cOmplete™), centrifuged for 20 min at 18,000 *g* and the supernatant was collected. 15 μg of whole cell lysate was separated on 4–12% Bis–Tris gels (NuPAGE™, Invitrogen) gels by SDS-PAGE and transferred onto nitrocellulose membranes (Millipore). For deglycosylation, lysates were treated with PNGaseF (New England Biolabs, Frankfurt, Germany) (500 U per 15 μg of protein) and incubated at 37 °C for 60 min prior to SDS-PAGE. For a detailed description of all primary and secondary antibodies, see Suppl. Spreadsheet S5.

2.13. Immunocytochemistry analysis

Cultured primary mouse brain endothelial cells were immunostained as described previously (Storck et al., 2021). Briefly, confluent cells were washed with TBS, fixed with ice-cold methanol for 10 min and RT acetone for 1 min. Unspecific binding of antibodies was blocked by incubating cells with 5% normal goat serum (Gibco) and 1% BSA in TBS for 60 min. Cells were incubated with primary antibodies overnight at 4 °C. Next day cells were washed briefly with TBS, incubated with secondary antibodies for 1 hr at RT and counterstained with DAPI. Images were acquired using LSM710 confocal microscope (Zeiss, Jena, Germany) and analysed with ImageJ software.

Mouse microvessels retained at the 40 μm strainer's mesh were fixed with 4% formaldehyde for 10 min and collected in 1% BSA in PBS by centrifugation at 4000 *g* for 20 min at 4 °C. Next, microvessels were permeabilized and immunostained as described above.

2.14. Immunohistochemistry analysis

Transcardial perfusion, sectioning and immunostaining of mouse brain slices was performed as described previously (Mazura et al., 2022), excluding the formic acid antigen retrieval.

2.15. Antibody radiolabelling and transport assays

For transport assays, rabbit polyclonal antibody (pAb) against SLC7A1 (Origene) and non-specific mouse IgG were radiolabelled using 10 μCi [^{125}I] radionuclide (PerkinElmer, Rodgau, Germany) in Pierce™ Iodination Tubes (ThermoFisher, Darmstadt, Germany), according to the Chizzonite indirect iodination manufacturer's protocol. Radiolabelled antibodies were then purified using desalting NAP™-5 columns (Cytiva, Freiburg, Germany) and the concentration was determined with the BCA assay. HCT116 and HCT116 *SLC7A1* KO cells were seeded in poly D-lysine coated 6-well plate at density 3×10^5 cells per well. Approximately 90% confluent cells were serum-starved for 1 h prior to internalisation assay. Cells were incubated with 3 μg/mL radiolabelled antibodies in serum-free media for 90 min, washed 3 times with PBS and PBS pH 2 to dissociate surface-bound antibodies. Next, cells were lysed with 0.2 M NaOH and lysates were subjected to protein precipitation using 10% 2,2,2-trichloroacetic acid (TCA). After 10 min incubation on ice, lysates were centrifuged at 20,000 *g* for 20 min at 4 °C. Supernatant containing unbound [^{125}I] was discarded and TCA-pellets were measured using the Wallac Wizard^2 2470 automatic γ-counter (PerkinElmer).

Confluent primary brain endothelial cells were subjected to transcytosis assay as described previously (Pflanzner et al., 2011). Briefly, to study blood-to-brain transport, serum-free media containing 30 μg/mL of radiolabelled [^{125}I] SLC7A1 antibody or non-specific mouse IgG and 1 μCi/mL [^{14}C] inulin (5 – 5.5 kDa) (PerkinElmer, Rodgau, Germany) was added to the luminal compartment of the Transwell. Cells were incubated for 90 min at 37 °C and intact [^{125}I] SLC7A1 antibody or mouse IgG was measured in both luminal and abluminal compartments. For that purpose, supernatants from both compartments were supplemented with 10% TCA and centrifuged at 20,000 *g* for 20 min at 4 °C. Supernatant containing unbound [^{125}I] was discarded and TCA-pellets were measured using γ-counter. Fraction of media not precipitated with TCA was used to analyze [^{14}C] via the Tri-Carb 2800 TR Liquid Scintillation Analyzer (PerkinElmer). The transcytosis quotient (TQ) of SLC7A1 antibody was calculated according to the formula SLC7A1 TQ = ([^{125}I] – SLC7A1 abluminal/[^{125}I] – SLC7A1 input)/([^{14}C] – inulin

abluminal/[^{14}C] − inulin input).

2.16. Alexa fluorophore-labelling and transcytosis in hCMEC/D3 cells

Immortalised human brain capillary endothelial cells (hCMEC/D3) were cultured in EBM2 culture medium (CC-3156) supplemented with EGM-2 SingleQuots (CC-4176, both from Lonza, Basel, Switzerland). For transcytosis, cells (passage 8–10) were seeded in 24-well Transwell filters at the density of 8×10^4 cells per well. Transendothelial electric resistance (TEER) and capacitance were monitored with cellZscope® system as described above. Rabbit IgG isotype control (Invitrogen) and rabbit polyclonal anti-SLC7A1 antibody (Origene) were labelled with Alexa Fluor 647 using the ReadyLabel™ Antibody Labeling Kit (Invitrogen) according to the manufacturer's protocol. The protein concentration was determined with NanoDrop One UV-Vis spectrophotometer (ThermoFisher). FITC-Dextran (3–4 kDa) (#53557, Sigma) was used as a control for paracellular diffusion. For transcytosis FITC-Dextran and respective antibodies were diluted in FluoroBrite™ DMEM (#A18967–01, Gibco) to the final concentration of 30 μg/mL and 100 μL of the antibody/Dextran solution was introduced to each Transwell representing luminal compartment of the BBB model in vitro. Fluorescence signal from luminal and abluminal compartments was detected at three time points (t_1= 0 min, t_2= 60 min, t_3 = 180 min) using Varioskan LUX Multimode Microplate Reader (ThermoFisher) and SkanIt Software 6.0.2. Transcytosis quotient was calculated as described above.

2.17. Statistical analysis

All experiments were repeated several times using multiple preparations of brain endothelial cells. Data with the number of sample units and independent experimental runs, indicated in each figure legend, are depicted as mean ± SD. If necessary, data normalization was conducted as described in the respective figure legend. All statistical analyses were carried out using the GraphPad Prism 8.4.3 software (La Jolla, CA, USA). To assess data distribution, Shapiro-Wilk normality test was performed. Unpaired Student's *t*-test was used for two groups comparisons. Statistical significance between groups was defined as $p < 0.05$ (*), $p < 0.01$ (**) or $p < 0.001$ (***). Final images and schematics were created using BioRender.com and CorelDRAW2022.

3. Results

3.1. Transcriptomic-based selection of brain endothelium-enriched genes

Bulk RNA-seq data from human primary endothelial cells from three tissues (brain, liver and lung) were analysed to identify genes enriched in brain endothelial cells compared to the other two tissue types (Fig. 1). Future validation experiments of BBB-TT would include various mouse models and therefore we added a mouse single-cell RNA-seq dataset in the initial screening process (He et al., 2018). Genes were identified with a higher expression in endothelial cells compared to either lung endothelial cells or other brain cell types (Suppl. Spreadsheet S2 and S3). The genes from those four comparisons were filtered by keeping one-to-one

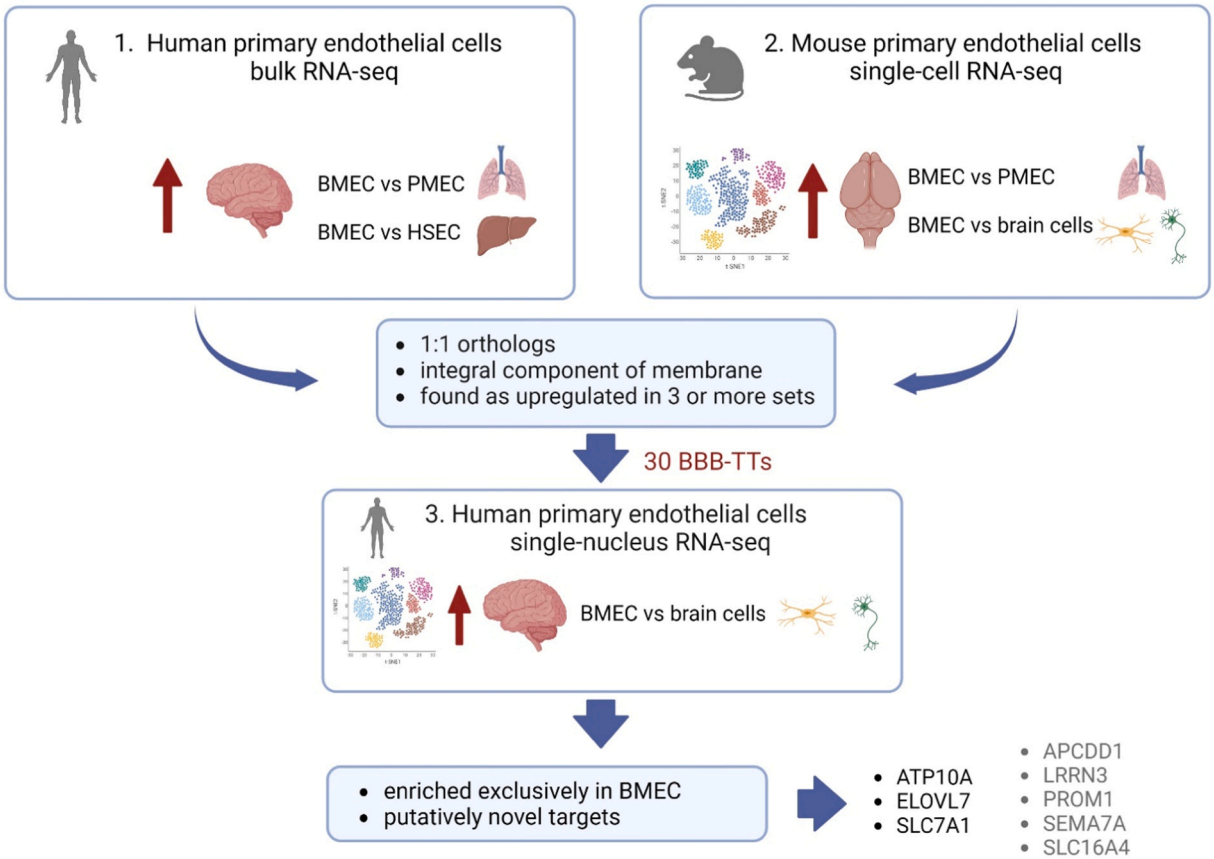

Fig. 1. Overview of transcriptomic selection workflow. Three RNA seq-based transcriptomic datasets were used to select an initial list of candidate genes encoding for blood-brain barrier transporters. Gene enrichment in human brain microvessels endothelial cells (BMEC) was compared to enrichment in human pulmonary or hepatic sinusoidal endothelial cells (PMEC and HSEC accordingly) as well as to other brain cells. Additionally, transcriptomic dataset of mouse single-cell RNA-seq analysis was included in the initial screening process. Out of 30 pre-selected candidates, eight BBB transport targets (BBB-TT; bottom right) were chosen. Genes listed in grey represent genes not found as being enriched in the human single-nucleus RNA-seq data, but found most consistently across the four main transcriptomic comparisons. Figure created with Biorender.com.

orthologs between humans and mice, broadly selecting for their functional annotation as integral components of the membrane (Gene ontology cellular component GO:0016021) and selecting consistent hits found in at least three comparisons. This selection approach resulted in an initial list of 30 target genes (Suppl. Spreadsheet S6).

A third single-nuclei transcriptomic dataset was used to further prioritize potential BBB-TT using its high resolution of specific cell types not available in the bulk data. RNA was obtained from enriched brain microvessels extracted from two samples of human frozen post-mortem frontal cortex tissue (see *Methods* section for details). The population of endothelial nuclei representing approximately 4% of all quality-filtered nuclei (101 nuclei) was used to investigate whether initial screening targets were enriched in those cells. Nine out of the 30 initial targets showed a significantly higher expression in brain endothelial nuclei compared to the remaining nuclei of all other brain cell types. Although being enriched in brain endothelium, a number of these nine genes were excluded: *SLCO2B1* was also enriched in microglia; *SGPP2* was also enriched in excitatory neurons; genes encoding solute carriers *SLC2A1* and *SLC7A5* have already been described and studied as BBB transporters (Patching, 2017; Puris et al., 2020); *OCLN* involved in the formation and regulation of tight junctions does not represent an adequate transporter. The three genes with the highest fold change in human brain endothelial cells compared to all other brain cell types were selected for additional prioritization and characterization: *ATP10A*, *ELOVL7* and *SLC7A1*. Additionally, five genes found in all four initial comparisons, which have not been studied elsewhere, were chosen for downstream analysis despite lacking enrichment in human snRNA-seq data: *APCDD1*, *LRRN3*, *PROM1*, *SEMA7A* and *SLC16A4*. Notably, all of those eight genes have been identified as BBB-enriched in a comprehensive mouse study of endothelial cells from multiple tissues (Munji et al., 2019).

3.2. Criteria selection panel

Eight pre-selected BBB-TT: ATP10A, APCDD1, ELOVL7, LRRN3, PROM1, SEMA7A, SLC16A4 and SLC7A1 were subjected to evaluation based on a three-stage selection panel established by us (Fig. 2). Each of the potential targets was scored on a 0–5–10 scale according to pre-selected criteria (Suppl. Spreadsheet S7). In the first stage, gene and protein expression in the endothelium as well as the subcellular localization were defined as *kill criteria* with a minimum threshold score of 25 out of 50. Initially, a stringent rule on *kill criteria* was applied, i.e., if the target scores 0 for any of these criteria, it should be excluded from further analysis. In the second stage, the screening was based on primary and secondary criteria, such as function in health and availability of transgenic models or ligands. Secondary criteria were only considered when two BBB-TT scored equally. Finally, a Strengths/ Weaknesses/ Opportunities/ Threats (SWOT) analysis was performed to make the final assessment. SLC7A1 scored the highest and was the only target that passed the *kill criteria* based on the stringent rule, i.e., with no 0 scores. ATP10A, APCDD1 and SLC16A4 were other targets passing the 25-point threshold, though each with one criterion scoring 0. Based on the evaluation of primary and secondary criteria, SLC7A1 and ATP10A were ranked as the top two candidates. Taking together transcriptomic analysis and downstream evaluation, we performed the SWOT analysis of SLC7A1, ATP10A and APCDD1 (Suppl. Spreadsheet S8). We found significantly more weaknesses and threats for ATP10A and APCDD1 than SLC7A1. *Apcdd1* expression was found to be downregulated in adult mice (Mazzoni et al., 2017). Importantly, analysis of *APCDD1* mRNA expression did not show enrichment in human brain endothelium (Zhang et al., 2016). The major problem concerning ATP10A is its relatively short extracellular domains (< 30 amino acids long) which might significantly constrict the drug design as well as binding and transcytosis of potential therapeutics. Moreover, ATP10A has a lower identity between human and mouse protein sequences compared to SLC7A1 (80% and 86% respectively). We did not find any mass

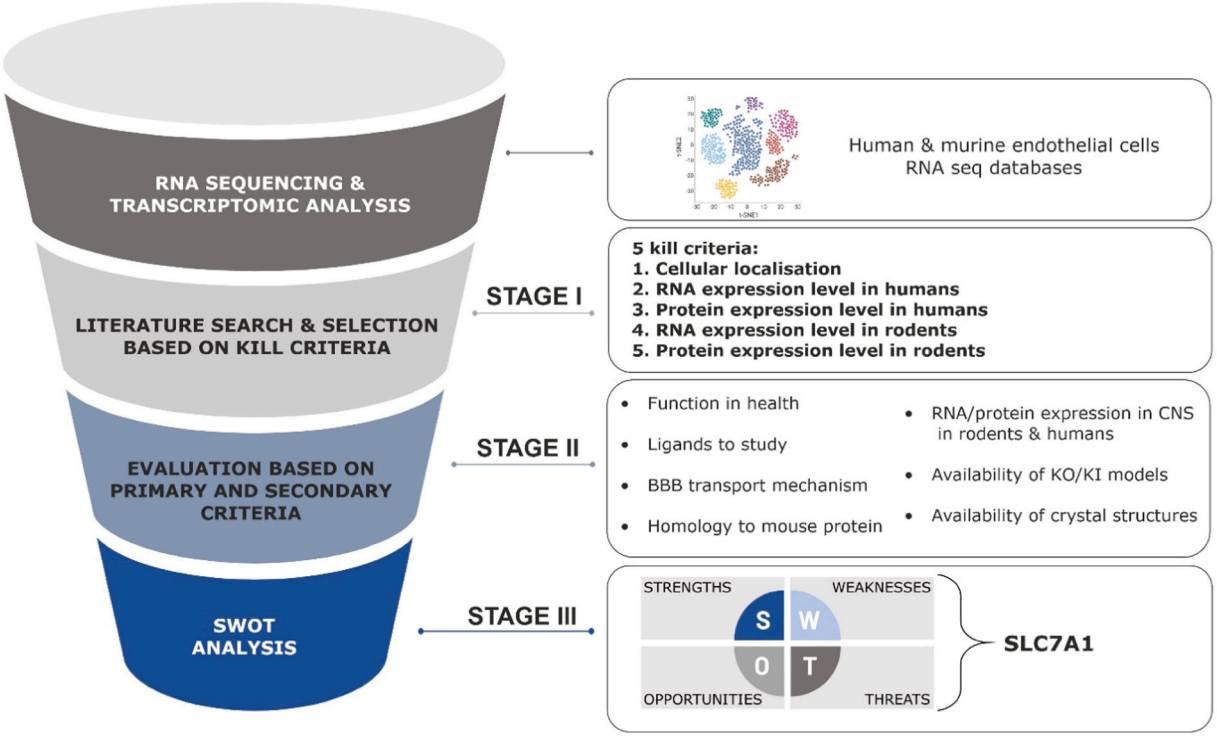

Fig. 2. Established workflow on prioritization and selection of potential novel BBB transport targets. A three-staged criteria panel was created to facilitate the screening of new targets enriched in single-nucleus RNA-seq of human brain microvascular endothelial cells. A score of 0, 5 or 10 points was assigned for each criterion. Candidates with the highest score were subjected to SWOT analysis for the final assessment. Figure created with BioRender.com.

spectrometry data related to ATP10A and SLC7A1 protein levels in the murine brain, however, SLC7A1 was confirmed by several groups in rat brain (Al Feteisi et al., 2018; Puris et al., 2022). ATP10A remains under-studied with no discovered protein function at the BBB or any other vascular bed. As a result, we selected and validated SLC7A1 as a novel potential transporter candidate in the in vitro and ex vivo studies.

3.3. *SLC7A1 gene expression in murine and human brain cortex*

After selecting SLC7A1 as a final BBB-TT, we performed ISH assay to compare *SLC7A1* distribution in the murine and human brain. Age-dependent changes in *Slc7a1* expression were previously reported in rats (Tachikawa et al., 2018), therefore both young (3-month-old) and old (2-year-old) WT C57BL/6 J mice were included in the study. In WT mice, we reported *Slc7a1* mRNA expression in the Platelet endothelial cell adhesion molecule 1 *(Pecam1)*-positive vessels of both young and old animals (Fig. 3A and B). Moreover, to analyse whether *SLC7A1* expression in humans in potentially dysregulated during neurodegenerative diseases, we used *SLC7A1* and *PECAM1*-specific mRNA probes and detected *SLC7A1* mRNA expression in the *PECAM1*-positive cortical vasculature of non-demented individuals as well as AD patients (Braak stage 6) (Fig. 3C and D). In accordance with previous reports (Yang et al., 2022), *PECAM1*-negative cells also showed substantial levels of *SLC7A1* mRNA, indicating that *SLC7A1* expression is not limited to the vasculature but can be detected in other cells of the CNS.

3.4. *SLC7A1 is expressed in human and mouse brain endothelial cells*

To determine SLC7A1 protein level in mouse brain endothelium, we first validated specificity of commercial antibodies targeting both extracellular and intracellular sites of SLC7A1 by Western blot (Suppl. Fig. S3). For this purpose, we used human embryonic kidney cells overexpressing *SLC7A1* (HEK *SLC7A1* WTOE) and human colorectal carcinoma cells with *SLC7A1* knock-out (HCT116 *SLC7A1* KO) cells generously provided by the IMI2 RESOLUTE consortium (Wiedmer et al., 2022). The mouse monoclonal antibody (Abnova, #H00006541-M02) showed a specific signal for SLC7A1 protein in HEK293T, HEK *SLC7A1* WTOE and HCT116 cells but not in HCT116 *SLC7A1* KO cells, as expected. Similarly, the rabbit pAb (Origene, #TA334048) detected SLC7A1 in these cells. However, it also showed weak signal in knock-out cells which might be due to a minor SLC7A1 expression leakage or reduced specificity of the polyclonal antibody. The Abnova antibody detected double bands in SLC7A1 expressing cells, corresponding to glycosylated and deglycosylated forms of SLC7A1 (Suppl. Fig. S2B) as supported by a study of Wang and colleagues who reported glycosylation of the third extracellular loop of SLC7A1 (Tachikawa et al., 2018). We therefore used both antibodies in further studies the Abnova antibody showed very high specificity, while Origene's antibody due to its binding to the extracellular site of SLC7A1, may serve as a suitable tool for further transport studies.

Next, we examined SLC7A1 protein expression in several epithelial and endothelial cell lines, commonly used as BBB in vitro models. We found that both mouse embryonic fibroblasts (MEF) and isolated primary murine brain microvascular endothelial cells (MBMEC) expressed SLC7A1, however no expression was detected in immortalized mouse brain endothelioma cells (bEnd.3), Chinese hamster ovary (CHO K1) cells, nor in the murine liver lysate (Fig. 4A). The latter two were used as a negative control as lack of SLC7A1 protein expression in CHO K1 and hepatic tissue was previously reported (Bai et al., 2019; Closs et al., 1997). Moreover, we could confirm SLC7A1 protein expression in the immortalised human brain capillary endothelial cell line (hCMEC/D3) reported by Watson and colleagues (Watson et al., 2016) (Fig. 4B). Recognition of SLC7A1 by the commercial antibodies used in this study was a prerequisite for the transcytosis studies in these cells.

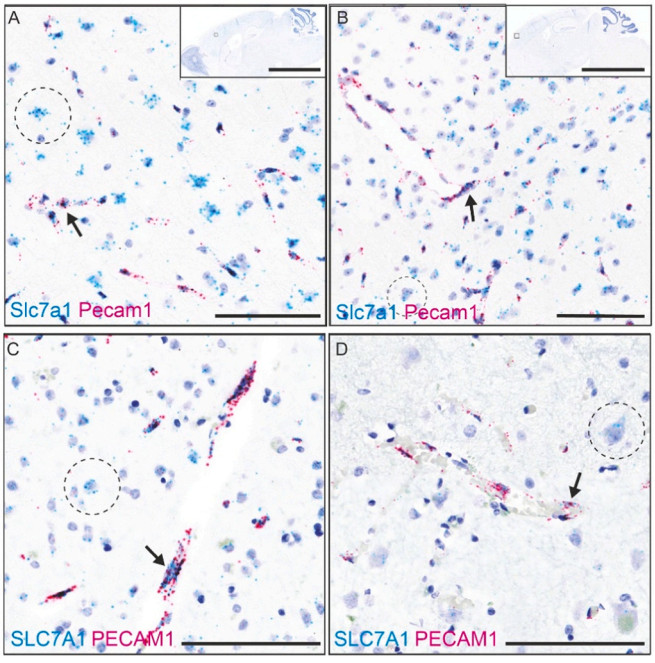

Fig. 3. In situ hybridization in brain cortex. A) Expression of *Slc7a1* mRNA in brain from 3-month-old mice. B) Expression of *Slc7a1* mRNA in brain from 2-year-old mice. C) *SLC7A1* mRNA expression in the human brain cortex from non-demented individuals. D) *SLC7A1* mRNA expression in brain cortex from AD patients. *Slc7a1/SLC7A1* visualized in teal and *Pecam1/PECAM1* in magenta. Cell nuclei were counterstained with haematoxylin. n=3/group. Scale bars represent 100 μm in the high magnification image and 5 mm in the overview images. Arrows indicate double-positive cells, dashed circles indicate cells only positive for *Slc7a1/ SLC7A1*.

3.5. *SLC7A1 protein distribution in the mouse brain*

Furthermore, we investigated SLC7A1 protein distribution in the mouse brain using the immunofluorescence assay. SLC7A1 could be clearly detected in the cortical vasculature (Fig. 5A), although not all the vessels showed SLC7A1 expression which is in line to our ISH results. The expression of SLC7A1 in other brain cells was under the detection level, similarly to IHC studies on human brain tissue (Suppl. Spreadsheet S7: SLC7A1 scoring). To further determine SLC7A1 expression within the neurovascular unit, we isolated brain microvessels from adult mice and performed immunostaining. As expected, we detected SLC7A1 in isolated capillaries as showed by co-staining with lectin (Fig. 5B). Again, SLC7A1 showed partial colocalization with the endothelium as demonstrated by the endothelial marker PECAM1.

3.6. *SLC7A1 mediates internalization and transport of specific anti-SLC7A1 antibody in vitro*

To evaluate SLC7A1 as a functional transporter, we first performed an internalization study in HCT116 cells expressing endogenous SLC7A1. As demonstrated in Fig. 6A, HCT116 effectively internalized SLC7A1-specific antibody as compared to HCT116 *SLC7A1* KO cells. Having confirmed the ability of SLC7A1 to internalize the antibody, we investigated whether SLC7A1 can effectively transport the antibody from luminal to abluminal side in brain endothelial cells derived from humans and mice. To do so, we isolated BMEC from adult mice, cultured them in a transwell system until cells reached a complete confluency and performed a transcytosis assay using 30 μg/mL radiolabelled [^{125}I]-SLC7A1 antibody for 90 min. Immediately after the incubation, we measured the amount of 2,2,2-trichloroacetic acid (TCA) precipitable radioactivity in the abluminal compartment, representing antibody-bound radioactivity transported across the endothelial cell monolayer. Endothelial cells exposed to [^{125}I]-SLC7A1 after 90 min exhibited a

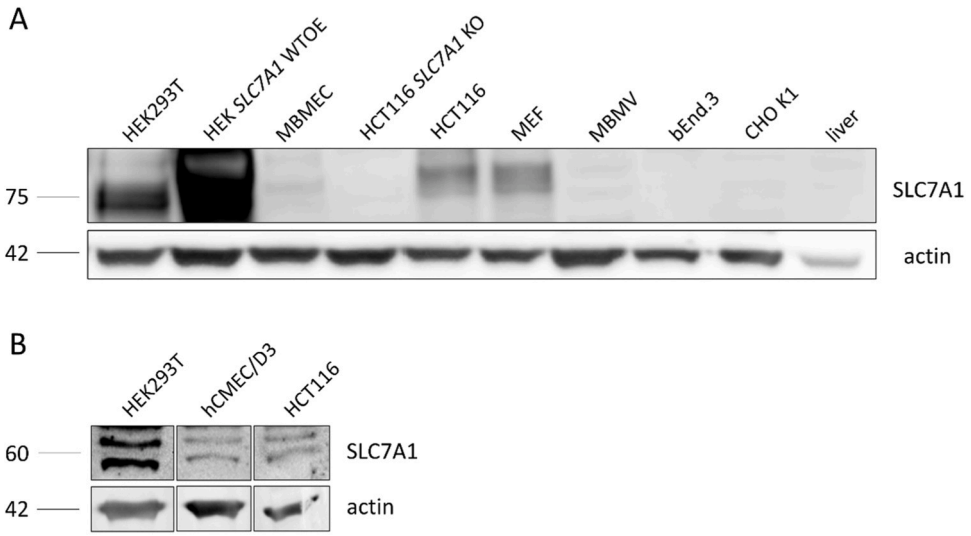

Fig. 4. SLC7A1 protein expression in various BBB in vitro models. (A) SLC7A1 expression can be detected in both isolated mouse brain microvascular endothelial cells (MBMEC) and mouse embryonic fibroblasts (MEF) but not in the immortalized mouse brain endothelioma cell line (bEnd.3). SLC7A1 expression in mouse brain microvessels (MBMV) is weaker compared to MBMEC, indicating the endothelium-specific SLC7A1 enrichment. Human embryonic kidney cells (HEK293T and HEK *SLC7A1* WTOE) and human colorectal cancer cells (HCT116) served as positive controls. Chinese hamster ovarian cells (CHO K1) and murine whole liver lysate served as negative controls, based on previously reported findings. No SLC7A1 expression was detected in HCT116 *SLC7A1* KO cells. (B) Verified SLC7A1 protein expression in the immortalised human brain capillary endothelial cell line (hCMEC/D3). All cell lysates were analysed on the same Western blot but rearranged for clearer presentation. β-actin used as a loading control. KO – knock out; WTOE – wild-type overexpressing.

three times higher transcytosis rate compared to cells treated with [^{125}I] -labelled non-specific mouse IgG (Fig. 6B, left). To account for paracellular transport, [^{14}C]-inulin was used and the transcytosis quotient (TQ) was calculated as described before (Pflanzner et al., 2011). No differences between groups were observed in [^{14}C]-inulin levels on the abluminal side, indicating similar rate of paracellular diffusion in both groups (Fig. 6B, right). Moreover, TEER and capacitance values indicated tight monolayer formation and did not show significant differences between the groups (Fig. 6C). For cross validation of the transcytosis, transport experiments have been repeated using fluorophore-labelled antibodies, confirming the initial results (see: Suppl. Fig. S4).

Finally, we performed a transcytosis study in the hCMEC/D3 cells, which are the most extensively characterised immortalised brain endothelial cells of human origin. hCMEC/D3 are routinely used for in vitro transport experiments as they sustain the brain endothelium phenotype including TJ formation, restrictive permeability to small compounds and apico-basal polarization (Tai et al., 2009; Weksler et al., 2013). hCMEC/D3 cells incubated with the Alexa fluor 647-conjugated SLC7A1 antibody for 60 min showed significantly higher fluorescence intensity measured in the apicobasal compartment compared to cells treated with the IgG isotype control (Fig. 6D). The observed effect was even more prominent after 180 min, indicating that SLC7A1 transporter effectively internalised the specific SLC7A1 antibody and transported it to the abluminal side. Importantly, the analysis of FITC-Dextran fluorescent signal measured in the abluminal compartment did not reveal any significant differences between the groups, excluding differences in paracellular diffusion as a contributing factor.

4. Discussion

In this study, we have established a unique workflow for prioritization and selection of potential novel transporters at the BBB. The three-stage analysis investigated multiple criteria such as gene and protein expression levels in rodents and humans, cellular localization, known ligands and/or inhibitors. This multilevel prioritization, combining both literature as well as transcriptomic and proteomic data, streamlined the selection and evaluation of a novel target. As a result, we selected the SLC7A1 transporter as a potential BBB transport target. SLC7A1, encoded by the *SLC7A1* gene, belongs to the solute carrier (SLC) superfamily transporting essential polar molecules such as glucose, amino acids and small peptides (Abbott et al., 2010; Helms et al., 2020). Few of the BBB-enriched SLC transporters: glucose transporter 1 (GLUT1 alias SLC2A1) and large neutral amino acids transporter (LAT1; heterodimer composed of SLC3A2 and SLC7A5) and basigin (SLC7A11) were previously investigated for the antibody delivery to the brain (Anraku et al., 2017; Christensen et al., 2021; Edavettal et al., 2022; Geier et al., 2013; Zhao et al., 2018; Zuchero et al., 2016), however, most of the SLC group members remain little studied. Being a functional amino acid transporter, SLC7A1 was reported as expressed in all tissues other than the liver, yet with varying abundance (Closs et al., 2006; Devés and Boyd, 1998). In endothelial cells, SLC7A1 is expressed at the plasma membrane, both at the luminal and abluminal side of the brain endothelium (He et al., 2014; Zlokovic, 2008). SLC7A1 provides the L-arginine required for nitric oxide (NO) synthesis, thereby having an intermediary role in modulating vascular tone and blood flow (Gambardella et al., 2020). In a more recent study, endothelial SLC7A1 showed properties for binding the bovine leukemia virus, opening the opportunities for exploration of the BBB entry mechanisms (Bai et al., 2019). Furthermore, SLC7A1 was described as a new cell adhesion molecule maintaining BBB integrity (Guo et al., 2015). Protein expression of SLC7A1 was correlated with VE-cadherin at the intracellular junctions, whereas *SLC7A1* silencing with siRNA resulted in increased BBB permeability. In this work, we focused on another potential function of SLC7A1 at the BBB, namely, transport of larger substances to the brain.

Our analysis of both gene and protein levels confirmed high abundance throughout the CNS. *Slc7a1* expression in the murine cortex was similar to the broad brain expression of *Tfrc* (Suppl. Fig. S3), implicating that SLC7A1-targeted molecules could not only cross the BBB but also target neuronal cells within the brain parenchyma. Our uptake studies showed that SLC7A1 can internalise large molecules such as immunoglobulins. That is in line with previously published data showing the ability of SLC7A1 to internalize antibodies through a clathrin-dependent mechanism (Vina-Vilaseca et al., 2011). Moreover, our transcytosis studies in human and murine brain endothelial cells demonstrated that SLC7A1 is a functional transporter, able to shuttle a specific antibody

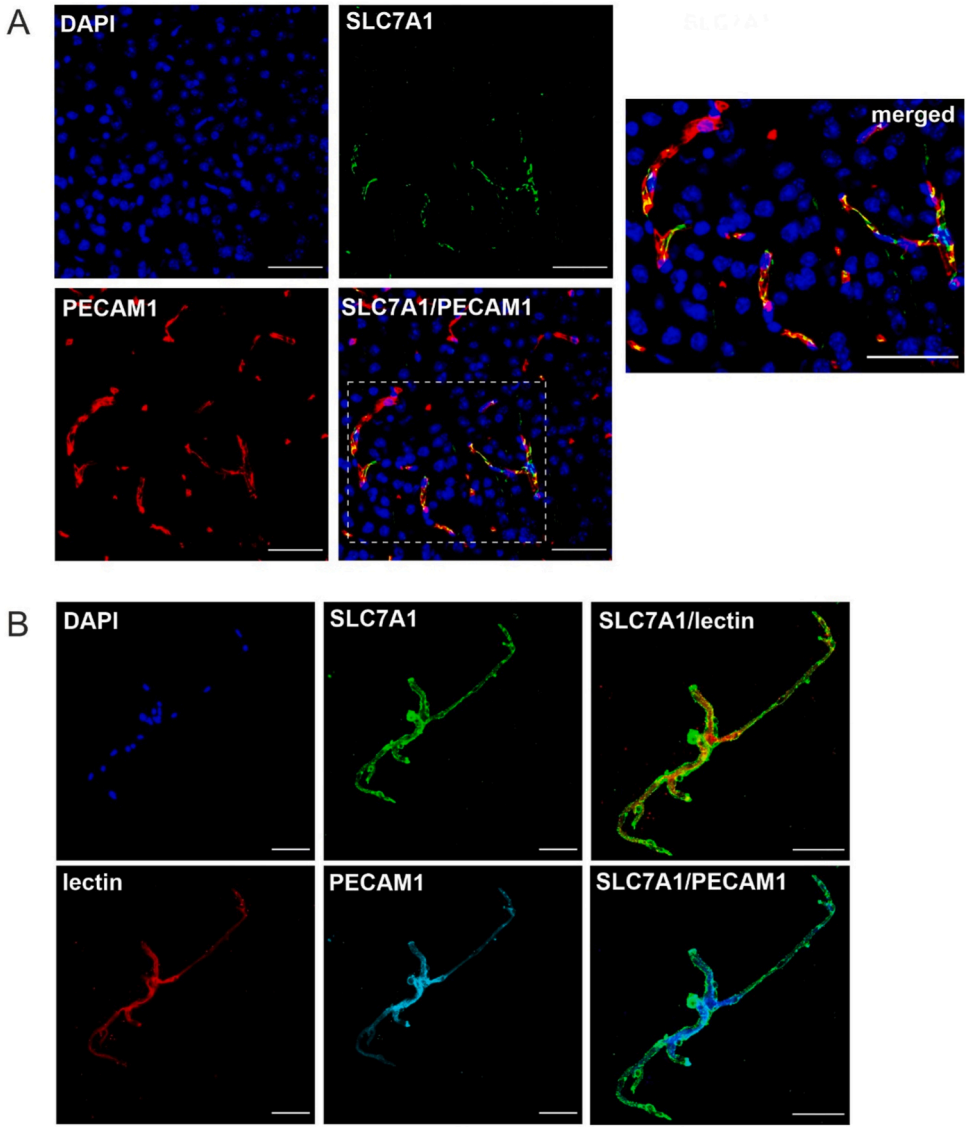

Fig. 5. SLC7A1 protein expression distribution in mouse brain tissue. A) SLC7A1 expression can be detected within the brain vasculature of the prefrontal cortex in 2-month-old wild-type mice. Scale bar = 50 μm. B) Partial co-localisation of SLC7A1 with vascular marker lectin and endothelial marker PECAM1 (CD31) in isolated murine brain microvessels. Scale bar = 50 μm. Nuclei counterstained with DAPI.

across the endothelium. Ideally, a transcytosis assay should be performed including a selective inhibitor of SLC7A1, yet no such molecule has been discovered. Novel tools such as nanobodies or small peptides binding to extracellular SLC7A1 domains are needed for further studies on SLC7A1 properties in vitro.

Currently, a scant number of receptors with the potential to deliver large molecules to the CNS have been tested in clinical trials and only several SLC6 inhibitors are being used in the treatment of depression and epilepsy (Giugliani et al., 2018; Kumthekar et al., 2020; Okuyama et al., 2019). The SLC superfamily includes over 450 proteins, heterogenous in structure, expression patterns and physiological functions, however, a substantial number of them remains understudied (Pizzagalli et al., 2021). A wealth of transcriptomic and proteomic data on BBB transporters has emerged in recent years thanks to the development of high-throughput genetic and biochemical assays (Garcia et al., 2022; Kalucka et al., 2020; Uchida et al., 2020; Winkler et al., 2022; Yang et al., 2022). Although the search for new delivery candidates is highly demanded, it must be supported by the use of pre-established selection criteria to narrow down the targets and thus facilitate the screening. Additionally, a potential discrepancy in expression levels of the receptor of interest in rodent and human brains have to be considered (Zhang et al., 2020). For this purpose, in this study we included RNA-seq data derived from both human and mouse samples. Moreover, we included AD patients' sample in the in situ hybridization assay as well as compared brain tissue derived from young and aged mice to explore whether SLC7A1 expression levels are altered during aging or neurodegeneration. Apart from a single study where SLC7A1 receptor endocytosis was investigated in aortic porcine endothelial cells (Vina-Vilaseca et al., 2011), there are no precedent studies exploring a potential of SLC7A1 as a transporter of large molecules. Here for the first time, we explore a potential of SLC7A1 to shuttle large biomolecules, such as mAbs, across the BBB.

The biggest limitation of using SLC7A1 as a specific transporter across the BBB might be its ubiquitous expression in peripheral organs (Closs et al., 2006). However, the same applies to the majority of investigated RMT family members, TFRC being the most studied (Pardridge, 2015). Transferrin (TF) is one of the most abundant plasma proteins and therefore expressed in most cell types, including endothelial cells of the brain microvasculature forming the BBB (Jefferies et al., 1984; Nairz and Weiss, 2020). High abundance of TF and vast TFRC

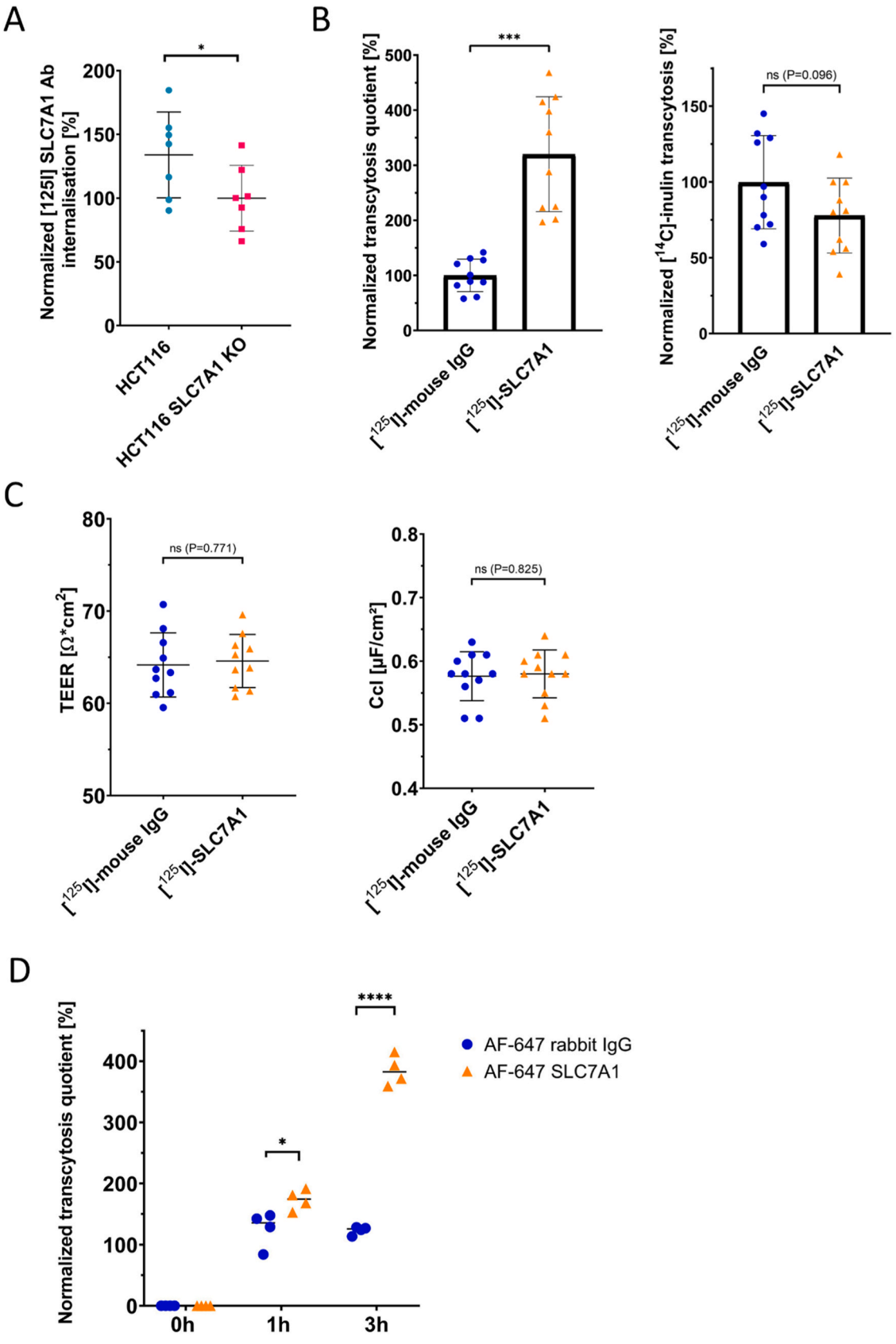

(caption on next page)

Fig. 6. Transport studies with specific anti-SLC7A1 antibody. (A) Internalisation assay in HCT116 cells. Cells were incubated for 90 min with 3 μg/mL [^{125}I] SLC7A1 antibody prior to lysis and TCA-precipitation. For statistical analysis unpaired one-tailed t-test was used (*p<0.05, **p<0.01, ***p<0.001). Data represent mean ± SD, n = 7/ group. Each datapoint represent one well. (B) Transcytosis assay in primary MBMEC. Functionality of SLC7A1 in primary MBMEC cultured for 6 days was analysed by transcytosis assay. Brain-to-blood transcytosis quotient (TQ) of anti-SLC7A1 antibody was three times higher compared to non-specific mouse IgG (left). TQ was normalized to paracellular transport of [^{14}C] inulin. Cells were treated with 30 μg/mL [^{125}I] SLC7A1 or [^{125}I] non-specific mouse IgG and 1 μCi/mL [^{14}C] inulin for 90 min before transcytosis analysis. No significant differences in inulin paracellular diffusion were observed between two groups (right). Data represent mean ± SD of n = 10/group. For statistical analysis unpaired two-tailed t-test was used (*p<0.05, **p<0.01, ***p<0.001). (C) Trans-endothelial electric resistance (left) and capacitance (right) measurements prior to the transcytosis assay confirm tight monolayer formation. Each data point represent one transwell. Data represent mean ± SD. (D) Transcytosis assay in immortalised human brain endothelial cell line. hCMEC/D3 cells were subjected to transcytosis assay with 30 μg/mL Alexa Fluor 647-conjugated SLC7A1 antibody (Origene) or rabbit IgG isotype control and equal amount of FITC-Dextran (3–4 kDa). Samples from the apical and basolateral compartment were analysed by fluorescence measurements at three time points. TQ was normalized to paracellular transport of low molecular weight FITC-Dextran. Data represent mean ± SD of n = 4/group. For statistical analysis unpaired two-tailed t-test was used (*p<0.05, **p<0.01, ***p<0.001, *** p<0.0001).

expression requires the administered TFRC-specific therapeutics to compete with endogenous TF for TFRC binding. The use of SLC7A1-specific antibodies might bring similar challenges. Fortunately, these concerns were addressed by researchers as well as pharmaceutical companies who developed several strategies to enhance antibody delivery to the brain. In case of TFRC targeting, antibodies binding to epitopes on the extracellular domain of TFRC distal to the TF binding site have been developed (Lajoie and Shusta, 2015). Other methods include conjugation or encapsulation in nanoparticles e.g. exosomes or liposomes (Bajracharya et al., 2021) or use of adeno-associated viruses with modified capsids enhancing their tropism for CNS penetration (Goertsen et al., 2022).

Recent publications have proven that a complex workflow of transcriptomic and proteomic studies is particularly fruitful in identification and validation of novel BBB-TT for delivery of large molecules into the CNS (Cegarra et al., 2022; Hill et al., 2021; Zuchero et al., 2016). Adapting a similar strategy and establishing unique criteria panel, we selected several novel candidates for BBB-TT, among which, SLC7A1 was evaluated as the most promising transporter. In this study, using various techniques, we confirmed that *SLC7A1* is expressed in murine and human brain endothelium. We also showed and confirmed in two independent laboratories that SLC7A1 is a functional transporter in isolated MBMEC. Our research uncovers the significant potential of the SLC7A1 as a novel and promising transporter of larger molecules. However, to fully harness and validate this potential, further comprehensive investigations, particularly in vivo, are warranted.

Ethics declarations

Approvals and permits for human tissue processing have been provided in appropriate paragraphs within the *Methods* section. Informed consent was obtained from all subjects involved in the study. All procedures involving animals were conducted in accordance with German (TierSchG 18.05.2006) and European (EU Directive 2010/63/EU) guidelines regarding the care and use of laboratory animals and were reviewed and approved (Ethical permit: 23 177–07/G 17–1–073) by the Central Animal Facility of the University of Mainz and the Ethics Committee on Animal Care and Use of Rheinland-Pfalz, Germany. In situ hybridization (ISH) experiments were conducted according to protocols approved by the Danish National Council for Animal Welfare (Ethical permit number: 2018–15–0201–01542). Reporting of the animal experiments complies with the ARRIVE guidelines 2.0 for how to report animal experiments.

Funding sources

This research was funded by the Innovative Medicines Initiative 2 Joint Undertaking (IMI2 JU), grant number 807015 (IM2PACT). The JU receives support from the European Union's Horizon 2020 research and innovation program and EFPIA. Funding for the present work was also supported by Novo Nordisk A/S, Janssen Pharmaceutica and Sanofi – all partners of IM2PACT consortium. The RESOLUTE project has received funding from IMI2 JU, grant number 777372. This Joint Undertaking receives support from the European Union's Horizon 2020 research and innovation program and EFPIA.

CRediT authorship contribution statement

Magdalena Kurtyka: Investigation, Formal Analysis, Visualization, Writing – original draft, Writing – review and editing. **Frank Wessely:** Investigation, Formal analysis, Visualization, Writing – original draft, Writing – review and editing. **Sarah Bau:** Investigation, Formal analysis, Visualization, Writing – original draft, Writing – review and editing. **Eseoghene Ifie:** Investigation, Formal analysis. **Liqun He:** Investigation, Formal analysis. **Nienke M de Wit:** Investigation, Formal analysis. **Alberte Bay Villekjær Pedersen:** Investigation, Formal analysis. **Maximilian Keller:** Investigation, Formal analysis, Visualization. **Caleb Webber:** Supervision, Funding acquisition. **Helga E de Vries:** Supervision, Funding acquisition, Writing – review & editing. **Olaf Ansorge:** Supervision, Funding acquisition. **Christer Betsholtz:** Supervision, Funding acquisition. **Marijke De Bock:** Investigation, Formal analysis. **Catarina Chaves:** Investigation, Formal analysis. **Birger Brodin:** Supervision, Funding acquisition. **Morten S Nielsen:** Supervision, Funding acquisition, Writing – review & editing. **Winfried Neuhaus:** Supervision, Funding acquisition. **Robert D Bell:** Investigation, Formal analysis. **Tamás Letoha:** Investigation, Formal analysis. **Axel H Meyer:** Investigation, Formal analysis. **Germán Leparc:** Investigation, Formal analysis. **Martin Lenter:** Investigation, Formal analysis. **Domnique Lesuisse:** Supervision, Writing – review & editing. **Zameel M Cader:** Supervision, Funding acquisition. **Stephen T Buckley:** Supervision. **Irena Loryan:** Supervision, Funding acquisition, Writing – original draft, Writing – review & editing. **Claus U Pietrzik:** Conceptualization, Supervision, Funding acquisition, Writing – review & editing.

Declaration of Competing Interest

The authors declare the following financial interests/personal relationships which may be considered as potential competing interests: Sarah Bau and Stephen T. Buckley are employees at Novo Nordisk. Catarina Chaves and Dominique Lesuisse are employees at Sanofi. Marijke De Bock is an employee at Janssen Pharmaceutica. Axel H. Mayer is an employee at AbbVie. German Leparc and Martin Lenter are employees at Boehringer Ingelheim Pharma. Tamas Letoha is the CEO of Pharmacoidea and Robert D. Bell is the Vice President and the Head of Research at Ascidian Therapeutics. All others declare no competing interests.

Data availability

Human primary endothelial cells RNA-seq data and post-mortem human brain microvessels-enriched single nucleus RNA-seq data are available from the NCBI Gene Expression Omnibus (GEO) via accession number: GEO SuperSeries GSE226607. Mouse brain and lung single-cell RNA-seq data are available from GEO via accession numbers GSE98816

and GSE99235, respectively. All remaining data is contained within the article or Supplementary Materials.

Acknowledgments

We would like to thank the EU IMI2 RESOLUTE consortium for providing the HEK and HCT116 *SLC7A1* WTOE and KO cell lines. We thank Colin Smith (University of Edinburgh) for providing the human brain cortex samples from non-demented individuals and AD patients as well as Oxford Genomics Centre at the Wellcome Centre for Human Genetics (funded by Wellcome Trust grant reference 203141/A/16/Z) for the generation and initial processing of the sequencing data.

Appendix A

References appearing in Suppl. Spreadsheet S7 but not in the main text: ("UniProt," n.d.), ("The Human Protein Atlas," n.d.), ("Brain RNA-Seq," n.d.),("Betsholtz Lab Vascular Single Cells RNA-seq Database," n.d.), ("The Biocompare Antibody Search Tool," n.d.), ("Basic Local Alignment Search Tool," n.d.), ("International Mouse Strain Resource," n.d.), ("The Jackson Laboratory," n.d.), ("Taconic Biosciences: Genetically Engineered Rodent Models," n.d.), (Perkins et al., 1997; Sato et al., 2020; Werner et al., 2019; (Jungnickel et al., 2018), (Takatsu et al., 2011; Chaudhry et al., 2015; "Patent Application TMEM30," n.d.), (Shimomura et al., 2010), ("Patent Application APCDD1 inhibitors," n.d.), (Halestrap, 2013; Jones and Morris, 2016; Keo et al., 2020; Purdy et al., 2015; Nie, L, 2020; Fukamachi et al., 2002; Gutiérrez-Franco et al., 2016; Xie and Wang, 2017; Sultana et al., 2012; Huang et al., 2019; Fargeas et al., 2015).

Supplementary materials

The following supporting information are available free of charge online: Suppl. Fig. S1: Endothelial phenotype validation and vascular nuclei isolation from frozen post-mortem brain tissue; Suppl. Fig. S2: Anti-SLC7A1 antibodies validation; Suppl. Fig. S3: In situ hybridization in brain cortex; Suppl. Fig. S4: Transcytosis assay with radiolabelled [^{125}I] SLC7A1 antibody (inter-lab cross validation). Suppl. Spreadsheet S1: List of human samples; Suppl. Spreadsheet S2: Comparison of mouse endothelial cells derived from brain versus lung tissue, Suppl. Spreadsheet S3: Comparison of mouse endothelial cells derived from brain versus other brain cells, Suppl. Spreadsheet S4: List of mRNA probes for in situ hybridization, Suppl. Spreadsheet S5: List of antibodies, Suppl. Spreadsheet S6: List of top 30 pre-selected targets, Suppl. Spreadsheet S7: Scoring of top eight pre-selected targets, Suppl. Spreadsheet S8: SWOT analysis of top three targets.

Appendix B. Supporting information

Supplementary data associated with this article can be found in the online version at doi:10.1016/j.ejcb.2024.151406.

References

Abbott, N.J., Patabendige, A.A.K., Dolman, D.E.M., Yusof, S.R., Begley, D.J., 2010. Structure and function of the blood-brain barrier. Neurobiol. Dis. 37, 13–25. https://doi.org/10.1016/j.nbd.2009.07.030.

Al Feteisi, H., Al-Majdoub, Z.M., Achour, B., Couto, N., Rostami-Hodjegan, A., Barber, J., 2018. Identification and quantification of blood–brain barrier transporters in isolated rat brain microvessels. J. Neurochem. 146, 670–685. https://doi.org/10.1111/jnc.14446.

Anraku, Y., Kuwahara, H., Fukusato, Y., Mizoguchi, A., Ishii, T., Nitta, K., Matsumoto, Y., Toh, K., Miyata, K., Uchida, S., Nishina, K., Osada, K., Itaka, K., Nishiyama, N., Mizusawa, H., Yamasoba, T., Yokota, T., Kataoka, K., 2017. Glycaemic control boosts glucosylated nanocarrier crossing the BBB into the brain. Nat. Commun. 8 https://doi.org/10.1038/s41467-017-00952-3.

Bai, L., Sato, H., Kubo, Y., Wada, S., Aida, Y., 2019. CAT1/SLC7A1 acts as a cellular receptor for bovine leukemia virus infection. FASEB J. . Publ. Fed. Am. Soc. Exp. Biol. 33, 14516–14527. https://doi.org/10.1096/fj.201901528R.

Bajracharya, R., Caruso, A.C., Vella, L.J., Nisbet, R.M., 2021. Current and emerging strategies for enhancing antibody delivery to the brain. Pharmaceutics 13, 1–16. https://doi.org/10.3390/pharmaceutics13122014.

Banks, W.A., 2016. From blood-brain barrier to blood-brain interface: New opportunities for CNS drug delivery. Nat. Rev. Drug Discov. 15, 275–292. https://doi.org/10.1038/nrd.2015.21.

Basic Local Alignment Search Tool [WWW Document], n.d. URL ⟨https://blast.ncbi.nlm.nih.gov/Blast.cgi⟩.

Bell, R.D., Winkler, E.A., Singh, I., Sagare, A.P., Deane, R., Wu, Z., Holtzman, D.M., Betsholtz, C., Armulik, A., Sallstrom, J., Berk, B.C., Zlokovic, B.V., 2012. Apolipoprotein e controls cerebrovascular integrity via cyclophilin A. Nature 485, 512–516. https://doi.org/10.1038/nature11087.

Ben-Zvi, A., Lacoste, B., Kur, E., Andreone, B.J., Mayshar, Y., Yan, H., Gu, C., 2014. MSFDA is critical for the formation and function of the blood brain barrier. Nature 509, 507–511. https://doi.org/10.1038/nature13324.MSFD2A.

Betsholtz Lab Vascular Single Cells RNA-seq Database [WWW Document], n.d. URL ⟨https://betsholtzlab.org/VascularSingleCells/database.html⟩.

Boado, R.J., Pardridge, W.M., 2017. Brain and organ uptake in the Rhesus monkey in vivo of recombinant iduronidase compared to an insulin receptor antibody-iduronidase fusion protein. Mol. Pharm. 14, 1271–1277. https://doi.org/10.1021/acs.molpharmaceut.6b01166.

Braak, H., Braak, E., 1991. Neuropathological stageing of Alzheimer-related changes. Acta Neuropathol. (Berl.) 82, 239–259. https://doi.org/10.1007/BF00308809.

Brain RNA-Seq [WWW Document], n.d. URL ⟨https://www.brainrnaseq.org/⟩.

Cegarra, C., Chaves, C., Déon, C., Do, T.M., Dumas, B., Frenzel, A., Kuhn, P., Roudieres, V., Guillemot, J.C., Lesuisse, D., 2022. Exploring ITM2A as a new potential target for brain delivery. Fluids Barriers CNS 19, 25. https://doi.org/10.1186/s12987-022-00321-3.

Chaudhry, M., Wang, X., Bamne, M.N., Hasnain, S., Demirci, F.Y., Lopez, O.L., Kamboh, M.I., 2015. Genetic Variation in Imprinted Genes is Associated with Risk of Late-Onset Alzheimer's Disease. J. Alzheimers Dis. 44, 989–994. https://doi.org/10.3233/JAD-142106.

Christensen, S.C., Hudecz, D., Jensen, A., Christensen, S., Nielsen, M.S., 2021. Basigin Antibodies with Capacity for Drug Delivery Across Brain Endothelial Cells. Mol. Neurobiol. 58, 4392–4403. https://doi.org/10.1007/s12035-021-02421-x.

Closs, E.I., Gräf, P., Habermeier, A., Cunningham, J.M., Förstermann, U., 1997. Human cationic amino acid transporters hCAT-1, hCAT-2A, and hCAT-2B: Three related carriers with distinct transport properties. Biochemistry 36, 6462–6468. https://doi.org/10.1021/bi962829p.

Closs, E.I., Boissel, J.P., Habermeier, A., Rotmann, A., 2006. Structure and function of cationic amino acid transporters (CATs). J. Membr. Biol. 213, 67–77. https://doi.org/10.1007/s00232-006-0875-7.

Devés, R., Boyd, C.A.R., 1998. Transporters for cationic amino acids in animal cells: Discovery, structure, and function. Physiol. Rev. 78, 487–545. https://doi.org/10.1152/physrev.1998.78.2.487.

Edavettal, S., Cejudo-Martin, P., Dasgupta, B., Yang, D., Buschman, M.D., Domingo, D., Van Kolen, K., Jaiprasat, P., Gordon, R., Schutsky, K., Geist, B., Taylor, N., Soubrane, C.H., Van Der Helm, E., LaCombe, A., Ainekulu, Z., Lacy, E., Aligo, J., Ho, J., He, Y., Lebowitz, P.F., Patterson, J.T., Scheer, J.M., Singh, S., 2022. Enhanced delivery of antibodies across the blood-brain barrier via TEMs with inherent receptor-mediated phagocytosis. Med 11, 1–23. https://doi.org/10.1016/j.medj.2022.09.007.

Fargeas, C.A., Büttner, E., Corbeil, D., 2015. Commentary: "Prom1 Function in Development, Intestinal Inflammation, and Intestinal Tumorigenesis. Front. Oncol. 5 https://doi.org/10.3389/fonc.2015.00091.

Feigin, V.L., Nichols, E., Alam, T., 2019. Global, regional, and national burden of neurological disorders, 1990–2016: a systematic analysis for the Global Burden of Disease Study 2016. Lancet Neurol. 18, 459–480. https://doi.org/10.1016/S1474-4422(18)30499-X.

Fukamachi, K., Matsuoka, Y., Ohno, H., Hamaguchi, T., Tsuda, H., 2002. Neuronal Leucine-rich Repeat Protein-3 Amplifies MAPK Activation by Epidermal Growth Factor through a Carboxyl-terminal Region Containing Endocytosis Motifs. J. Biol. Chem. 277, 43549–43552. https://doi.org/10.1074/jbc.C200502200.

Gambardella, J., Khondkar, W., Morelli, M.B., Wang, X., Santulli, G., Trimarco, V., 2020. Arginine and Endothelial Function. Biomedicines 8, 277. https://doi.org/10.3390/biomedicines8080277.

Garcia, F.J., Sun, N., Lee, H., Godlewski, B., Mathys, H., Galani, K., Zhou, B., Jiang, X., Ng, A.P., Mantero, J., Tsai, L.H., Bennett, D.A., Sahin, M., Kellis, M., Heiman, M., 2022. Single-cell dissection of the human brain vasculature. Nature 603, 893–899. https://doi.org/10.1038/s41586-022-04521-7.

Geier, E.G., Schlessinger, A., Fan, H., Gable, J.E., Irwin, J.J., Sali, A., Giacomini, K.M., 2013. Structure-based ligand discovery for the Large-neutral Amino Acid Transporter 1, LAT-1. Proc. Natl. Acad. Sci. U. S. A. 110, 5480–5485. https://doi.org/10.1073/pnas.1218165110.

Giugliani, R., Giugliani, L., De Oliveira Poswar, F., Donis, K.C., Corte, A.D., Schmidt, M., Boado, R.J., Nestrasil, I., Nguyen, C., Chen, S., Pardridge, W.M., 2018. Neurocognitive and somatic stabilization in pediatric patients with severe Mucopolysaccharidosis Type i after 52 weeks of intravenous brain-penetrating insulin receptor antibody-iduronidase fusion protein (valanafusp alpha): An open label phase 1-2 trial. Orphanet J. Rare Dis. 13, 1–11. https://doi.org/10.1186/s13023-018-0849-8.

Gklinos, P., Papadopoulou, M., Stanulovic, V., Mitsikostas, D.D., Papadopoulos, D., 2021. Monoclonal antibodies as neurological therapeutics. Pharmaceuticals 14, 1–31. https://doi.org/10.3390/ph14020092.

Goertsen, D., Flytzanis, N.C., Goeden, N., Chuapoco, M.R., Cummins, A., Chen, Yijing, Fan, Y., Zhang, Q., Sharma, J., Duan, Y., Wang, L., Feng, G., Chen, Yu, Ip, N.Y.,

Pickel, J., Gradinaru, V., 2022. AAV capsid variants with brain-wide transgene expression and decreased liver targeting after intravenous delivery in mouse and marmoset. Nat. Neurosci. 25, 106–115. https://doi.org/10.1038/s41593-021-00969-4.

Grubman, A., Chew, G., Ouyang, J.F., Sun, G., Choo, X.Y., McLean, C., Simmons, R.K., Buckberry, S., Vargas-Landin, D.B., Poppe, D., Pflueger, J., Lister, R., Rackham, O.J. L., Petretto, E., Polo, J.M., 2019. A single-cell atlas of entorhinal cortex from individuals with Alzheimer's disease reveals cell-type-specific gene expression regulation. Nat. Neurosci. 22, 2087–2097. https://doi.org/10.1038/s41593-019-0539-4.

Guo, L., Tian, S., Chen, Y., Mao, Y., Cui, S., Hu, A., Zhang, J., Xia, S.L., Su, Y., Du, J., Block, E.R., Wang, X.L., Cui, Z., 2015. CAT-1 as a novel CAM stabilizes endothelial integrity and mediates the protective actions of l-Arg via a NO-independent mechanism. J. Mol. Cell. Cardiol. 87, 180–191. https://doi.org/10.1016/j.yjmcc.2015.08.011.

Gutiérrez-Franco, A., Costa, C., Eixarch, H., Castillo, M., Medina-Rodríguez, E.M., Bribián, A., De Castro, F., Montalban, X., Espejo, C., 2016. Differential expression of sema3A and sema7A in a murine model of multiple sclerosis: Implications for a therapeutic design. Clin. Immunol. 163, 22–33. https://doi.org/10.1016/j.clim.2015.12.005.

Halestrap, A.P., 2013. The SLC16 gene family – Structure, role and regulation in health and disease. Mol. Asp. Med. 34, 337–349. https://doi.org/10.1016/j.mam.2012.05.003.

He, L., Vanlandewijck, M., Lebouvier, T., Mäe, M.A., Nahar, K., Betsholtz, C., 2018. Primary isolation of vascular cells from murine brain for single cell sequencing. Sci. Data 5.

He, Y., Yao, Y., Tsirka, S.E., Cao, Y., 2014. Cell-culture models of the blood-brain barrier. Stroke 45, 2514–2526. https://doi.org/10.1161/STROKEAHA.114.005427.

Helms, H.C.C., Kristensen, M., Saaby, L., Fricker, G., Brodin, B., 2020. Drug Delivery Strategies to Overcome the Blood–Brain Barrier (BBB). : Handb. Exp. Pharmacol. 151–183. https://doi.org/10.1007/164_2020_403.

Hill, J.J., Haqqani, A.S., Stanimirovic, D.B., 2021. Proteome of the Luminal Surface of the Blood–Brain Barrier. Proteomes 9, 45. https://doi.org/10.3390/proteomes9040045.

Hoheisel, D., Nitz, T., Franke, H., Wegener, J., Hakvoort, A., Tilling, T., Galla, H.-J., 1998. Hydrocortisone Reinforces the Blood–Brain Barrier Properties in a Serum Free Cell Culture System. Biochem. Biophys. Res. Commun. 244, 312–316. https://doi.org/10.1006/bbrc.1997.8051.

Huang, X., Wan, J., Leng, D., Zhang, Y., Yang, S., 2019. Dual-targeting nanomicelles with CD133 and CD44 aptamers for enhanced delivery of gefitinib to two populations of lung cancer-initiating cells. Exp. Ther. Med. https://doi.org/10.3892/etm.2019.8220.

International Mouse Strain Resource [WWW Document], n.d. URL ⟨https://www.findmice.org/⟩.

Jefferies, W.A., Brandon, M.R., Hunt, S.V., Williams, A.F., Gatter, K.C., Mason, D.Y., 1984. Transferrin receptor on endothelium of brain capillaries. Nature 312, 162–163. https://doi.org/10.1038/312162a0.

Johnsen, K.B., Burkhart, A., Thomsen, L.B., Andresen, T.L., Moos, T., 2019. Targeting the transferrin receptor for brain drug delivery. Prog. Neurobiol. 181, 101665 https://doi.org/10.1016/j.pneurobio.2019.101665.

Jones, R., Morris, M., 2016. Monocarboxylate Transporters: Therapeutic Targets and Prognostic Factors in Disease. Clin. Pharmacol. Ther. 100, 454–463. https://doi.org/10.1002/cpt.418.

Jungnickel, K.E.J., Parker, J.L., Newstead, S., 2018. Structural basis for amino acid transport by the CAT family of SLC7 transporters. Nat. Commun. 9 https://doi.org/10.1038/s41467-018-03066-6.

Kadry, H., Noorani, B., Cucullo, L., 2020. A blood–brain barrier overview on structure, function, impairment, and biomarkers of integrity. Fluids Barriers CNS 17 (1), 24. https://doi.org/10.1186/s12987-020-00230-3.

Kalucka, J., de Rooij, L.P.M.H., Goveia, J., Rohlenova, K., Dumas, S.J., Meta, E., Conchinha, N.V., Taverna, F., Teuwen, L.A., Veys, K., García-Caballero, M., Khan, S., Geldhof, V., Sokol, L., Chen, R., Treps, L., Borri, M., de Zeeuw, P., Dubois, C., Karakach, T.K., Falkenberg, K.D., Parys, M., Yin, X., Vinckier, S., Du, Y., Fenton, R. A., Schoonjans, L., Dewerchin, M., Eelen, G., Thienpont, B., Lin, L., Bolund, L., Li, X., Luo, Y., Carmeliet, P., 2020. Single-Cell Transcriptome Atlas of Murine Endothelial Cells. Cell 180, 764–779.e20. https://doi.org/10.1016/j.cell.2020.01.015.

Kariolis, M.S., Wells, R.C., Getz, J.A., Kwan, W., Mahon, C.S., Tong, R., Kim, D.J., Srivastava, A., Bedard, C., Henne, K.R., Giese, T., Assimon, V.A., Chen, X., Zhang, Y., Solanoy, H., Jenkins, K., Sanchez, P.E., Kane, L., Miyamoto, T., Chew, K.S., Pizzo, M. E., Liang, N., Calvert, M.E.K., DeVos, S.L., Baskaran, S., Hall, S., Sweeney, Z.K., Thorne, R.G., Watts, R.J., Dennis, M.S., Silverman, A.P., Zuchero, Y.J.Y., 2020. Brain delivery of therapeutic proteins using an Fc fragment blood-brain barrier transport vehicle in mice and monkeys. Sci. Transl. Med. 12, 1–14. https://doi.org/10.1126/scitranslmed.aay1359.

Keaney, J., Campbell, M., 2015. The dynamic blood-brain barrier. FEBS J. 282, 4067–4079. https://doi.org/10.1111/febs.13412.

Keo, A., Mahfouz, A., Ingrassia, A.M.T., Meneboo, J.-P., Villenet, C., Mutez, E., Comptdaer, T., Lelieveldt, B.P.F., Figeac, M., Chartier-Harlin, M.-C., Van De Berg, W. D.J., Van Hilten, J.J., Reinders, M.J.T., 2020. Transcriptomic signatures of brain regional vulnerability to Parkinson's disease. Commun. Biol. 3, 101. https://doi.org/10.1038/s42003-020-0804-9.

Kumthekar, P., Tang, S.C., Brenner, A.J., Kesari, S., Piccioni, D.E., Anders, C., Carrillo, J., Chalasani, P., Kabos, P., Puhalla, S., Tkaczuk, K., Garcia, A.A., Ahluwalia, M.S., Wefel, J.S., Lakhani, N., Ibrahim, N., 2020. ANG1005, a Brain-Penetrating Peptide–Drug Conjugate, Shows Activity in Patients with Breast Cancer with Leptomeningeal Carcinomatosis and Recurrent Brain Metastases. Clin. Cancer Res. 26, 2789–2799. https://doi.org/10.1158/1078-0432.CCR-19-3258.

Lajoie, J.M., Shusta, E.V., 2015. Targeting receptor-mediated transport for delivery of biologics across the blood-brain barrier. Annu. Rev. Pharmacol. Toxicol. 55, 613–631. https://doi.org/10.1146/annurev-pharmtox-010814-124852.

Leberer, E., Mastrobattista, E., 2022. Innovative Medicine Initiatives: COMPACT Project Factsheets. [Accessed: 23 December 2022] [WWW Document]. URL ⟨https://www.imi.europa.eu/projects-results/project-factsheets/compact⟩.

Lee, Y.K., Uchida, H., Smith, H., Ito, A., Sanchez, T., 2019. The isolation and molecular characterization of cerebral microvessels. Nat. Protoc. 14, 3059–3081. https://doi.org/10.1038/s41596-019-0212-0.

Love, M.I., Huber, W., Anders, S., 2014. Moderated estimation of fold change and dispersion for RNA-seq data with DESeq2. Genome Biol. 15, 1–21. https://doi.org/10.1186/s13059-014-0550-8.

Love, M.I., Soneson, C., Hickey, P.F., Johnson, L.K., Tessa Pierce, N., Shepherd, L., Morgan, M., Patro, R., 2020. Tximeta: Reference sequence checksums for provenance identification in RNA-seq. PLoS Comput. Biol. 16, 1–13. https://doi.org/10.1371/journal.pcbi.1007664.

Mathys, H., Davila-velderrain, J., Peng, Z., Gao, F., Young, J.Z., Menon, M., He, L., Abdurrob, F., Jiang, X., Martorell, A.J., Ransohoff, R.M., Hafler, B.P., 2019. Single-cell transcriptomic analysis of Alzheimer's disease. Nature 570, 332–337. https://doi.org/10.1038/s41586-019-1195-2.Single-cell.

Mazura, A.D., Ohler, A., Storck, S.E., Kurtyka, M., Scharfenberg, F., Weggen, S., Becker-Pauly, C., Pietrzik, C.U., 2022. PCSK9 acts as a key regulator of Aβ clearance across the blood–brain barrier. Cell. Mol. Life Sci. 79, 1–15. https://doi.org/10.1007/s00018-022-04237-x.

Mazzoni, J., Smith, J.R., Shahriar, S., Cutforth, T., Ceja, B., Agalliu, D., 2017. The Wnt Inhibitor Apcdd1 Coordinates Vascular Remodeling and Barrier Maturation of Retinal Blood Vessels. Neuron 96, 1055–1069.e6. https://doi.org/10.1016/j.neuron.2017.10.025.

Munji, R.N., Soung, A.L., Weiner, G.A., Sohet, F., Semple, B.D., Trivedi, A., Gimlin, K., Kotoda, M., Korai, M., Aydin, S., Batugal, A., Cabangcala, A.C., Schupp, P.G., Oldham, M.C., Hashimoto, T., Noble-Haeusslein, L.J., Daneman, R., 2019. Profiling the mouse brain endothelial transcriptome in health and disease models reveals a core blood–brain barrier dysfunction module. Nat. Neurosci. 22, 1892–1902. https://doi.org/10.1038/s41593-019-0497-x.

Nairz, M., Weiss, G., 2020. Iron in health and disease. Mol. Asp. Med. 75, 100906 https://doi.org/10.1016/j.mam.2020.100906.

Nie, L., 2020. Crystal structure of human ELOVL fatty acid elongase 7 (ELOVL7). RCSB PDB. ⟨https://doi.org/10.2210/pdb6Y7F/pdb⟩.

O'Keeffe, E., Campbell, M., 2016. Modulating the paracellular pathway at the blood–brain barrier: current and future approaches for drug delivery to the CNS. Drug Discov. Today Technol. 20, 35–39. https://doi.org/10.1016/j.ddtec.2016.07.008.

Okuyama, T., Eto, Y., Sakai, N., Minami, K., Yamamoto, T., Sonoda, H., Yamaoka, M., Tachibana, K., Hirato, T., Sato, Y., 2019. Iduronate-2-Sulfatase with Anti-human Transferrin Receptor Antibody for Neuropathic Mucopolysaccharidosis II: A Phase 1/2 Trial. Mol. Ther. 27, 456–464. https://doi.org/10.1016/j.ymthe.2018.12.005.

Okuyama, T., Eto, Y., Sakai, N., Nakamura, K., Yamamoto, T., Yamaoka, M., Ikeda, T., So, S., Tanizawa, K., Sonoda, H., Sato, Y., 2021. A Phase 2/3 Trial of Pabinafusp Alfa, IDS Fused with Anti-Human Transferrin Receptor Antibody, Targeting Neurodegeneration in MPS-II. Mol. Ther. 29, 671–679. https://doi.org/10.1016/j.ymthe.2020.09.039.

Pardridge, W.M., 2015. Blood-brain barrier drug delivery of IgG fusion proteins with a transferrin receptor monoclonal antibody. Expert Opin. Drug Deliv. 12, 207–222. https://doi.org/10.1517/17425247.2014.952627.

Pardridge, W.M., 2022. A Historical Review of Brain Drug Delivery. Pharmaceutics 14, 1283. https://doi.org/10.3390/pharmaceutics14061283.

Patching, S.G., 2017. Glucose Transporters at the Blood-Brain Barrier: Function, Regulation and Gateways for Drug Delivery. Mol. Neurobiol. 54, 1046–1077. https://doi.org/10.1007/s12035-015-9672-6.

Patent Application APCDD1 inhibitors [WWW Document], n.d. URL ⟨https://patentimages.storage.googleapis.com/62/47/4a/76870314731d81/EP2474556A2.pdf⟩ (accessed 7.16.23).

Patent Application TMEM30 [WWW Document], n.d. URL 10.3233/JAD-142106 (accessed 7.16.23).

Patro, R., Duggal, G., Love, M.I., Irizarry, R.A., Kingsford, C., 2017. Salmon provides fast and bias-aware quantification of transcript expression. Nat. Methods 14, 417–419. https://doi.org/10.1038/nmeth.4197.

Perkins, C.P., Mar, V., Shutter, J.R., Castillo, J.D., Danilenko, D.M., Medlock, E.S., Ponting, I.L., Graham, M., Stark, K.L., Zuo, Y., Cunningham, J.M., Bosselman, R.A., 1997. Anemia and perinatal death result from loss of the murine ecotropic retrovirus receptor mCAT-1. Genes Dev. 11, 914–925. https://doi.org/10.1101/gad.11.7.914.

Pflanzner, T., Janko, M.C., André-Dohmen, B., Reuss, S., Weggen, S., Roebroek, A.J.M., Kuhlmann, C.R.W., Pietrzik, C.U., 2011. LRP1 mediates bidirectional transcytosis of amyloid-β across the blood-brain barrier. Neurobiol. Aging 32, 2323.e1–2323.e11. https://doi.org/10.1016/j.neurobiolaging.2010.05.025.

Pizzagalli, M.D., Bensimon, A., Superti-Furga, G., 2021. A guide to plasma membrane solute carrier proteins. FEBS J. 288, 2784–2835. https://doi.org/10.1111/febs.15531.

Profaci, C.P., Munji, R.N., Pulido, R.S., Daneman, R., 2020. The blood–brain barrier in health and disease: Important unanswered questions. J. Exp. Med. 217, 1–16. https://doi.org/10.1084/jem.20190062.

Purdy, J.G., Shenk, T., Rabinowitz, J.D., 2015. Fatty Acid Elongase 7 Catalyzes Lipidome Remodeling Essential for Human Cytomegalovirus Replication. Cell Rep. 10, 1375–1385. https://doi.org/10.1016/j.celrep.2015.02.003.

Puris, E., Gynther, M., Auriola, S., Huttunen, K.M., 2020. L-Type amino acid transporter 1 as a target for drug delivery. Pharm. Res. 37, 88. https://doi.org/10.1007/s11095-020-02826-8.

Puris, E., Auriola, S., Petralla, S., Hartman, R., Gynther, M., De Lange, E.C.M., Fricker, G., 2022. Altered protein expression of membrane transporters in isolated cerebral microvessels and brain cortex of a rat Alzheimer's disease model. Neurobiol. Dis. 169, 105741 https://doi.org/10.1016/j.nbd.2022.105741.

Pyke, C., 2020. Automated ISH for validated Histological Mapping of Lowly Expressed Genes. Methods in Molecular Biology (Clifton, N.J.), in: Methods in Molecular Biology. Springer Protocols, pp. 219–228 https://doi.10.1007/978-1-0716-0623-0_14.

Ruck, T., Bittner, S., Epping, L., Herrmann, A.M., Meuth, S.G., 2014. Isolation of primary murine brain microvascular endothelial cells. J. Vis. Exp. 6–11. https://doi.org/10.3791/52204.

Sakamoto, K., Shinohara, T., Adachi, Y., Asami, T., Ohtaki, T., 2017. A novel LRP1-binding peptide L57 that crosses the blood brain barrier. Biochem. Biophys. Rep. 12, 135–139. https://doi.org/10.1016/j.bbrep.2017.07.003.

Satija, R., Farrell, J.A., Gennert, D., Schier, A.F., Regev, A., 2015. Spatial reconstruction of single-cell gene expression data. Nat. Biotechnol. 33, 495–502. https://doi.org/10.1038/nbt.3192.

Sato, H., Bai, L., Borjigin, L., Aida, Y., 2020. Overexpression of bovine leukemia virus receptor SLC7A1/CAT1 enhances cellular susceptibility to BLV infection on luminescence syncytium induction assay (LuSIA). Virol. J. 17, 57. https://doi.org/10.1186/s12985-020-01324-y.

Shimomura, Y., Agalliu, D., Vonica, A., Luria, V., Wajid, M., Baumer, A., Belli, S., Petukhova, L., Schinzel, A., Brivanlou, A.H., Barres, B.A., Christiano, A.M., 2010. APCDD1 is a novel Wnt inhibitor mutated in hereditary hypotrichosis simplex. Nature 464, 1043–1047. https://doi.org/10.1038/nature08875.

Storck, S.E., Meister, S., Nahrath, J., Meißner, J.N., Schubert, N., Di Spiezio, A., Baches, S., Vandenbroucke, R.E., Bouter, Y., Prikulis, I., Korth, C., Weggen, S., Heimann, A., Schwaninger, M., Bayer, T.A., Pietrzik, C.U., 2016. Endothelial LRP1 transports amyloid-β1-42 across the blood-brain barrier. J. Clin. Invest. 126, 123–136. https://doi.org/10.1172/JCI81108.

Storck, S.E., Kurtyka, M., Pietrzik, C.U., 2021. Brain endothelial LRP1 maintains blood–brain barrier integrity. Fluids Barriers CNS 18 (1), 7. https://doi.org/10.1186/s12987-021-00260-5.

Sultana, H., Neelakanta, G., Foellmer, H.G., Montgomery, R.R., Anderson, J.F., Koski, R. A., Medzhitov, R.M., Fikrig, E., 2012. Semaphorin 7A Contributes to West Nile Virus Pathogenesis through TGF-β1/Smad6 Signaling. J. Immunol. 189, 3150–3158. https://doi.org/10.4049/jimmunol.1201140.

Tachikawa, M., Hirose, S., Akanuma, S., Matsuyama, R., Hosoya, K., 2018. Developmental changes of L-arginine transport at the blood-brain barrier in rats. Microvasc. Res. 117, 16–21. https://doi.org/10.1016/j.mvr.2017.12.003.

Taconic Biosciences: Genetically Engineered Rodent Models [WWW Document], n.d. URL ⟨https://www.taconic.com/⟩.

Tai, L.M., Reddy, P.S., Lopez-Ramirez, M.A., Davies, H.A., Male, A.D.K., Loughlin, A.J., Romero, I.A., 2009. Polarized P-glycoprotein expression by the immortalised human brain endothelial cell line, hCMEC/D3, restricts apical-to-basolateral permeability to rhodamine 123. Brain Res 1292, 14–24. https://doi.org/10.1016/j.brainres.2009.07.039.

Takatsu, H., Baba, K., Shima, T., Umino, H., Kato, U., Umeda, M., Nakayama, K., Shin, H.-W., 2011. ATP9B, a P4-ATPase (a Putative Aminophospholipid Translocase), Localizes to the trans-Golgi Network in a CDC50 Protein-independent Manner. J. Biol. Chem. 286, 38159–38167. https://doi.org/10.1074/jbc.M111.281006.

The Biocompare Antibody Search Tool [WWW Document], n.d. URL ⟨https://www.biocompare.com/Search-Antibodies/⟩.

The Human Protein Atlas [WWW Document], n.d. URL ⟨https://www.proteinatlas.org/⟩.

The Jackson Laboratory [WWW Document], n.d. URL ⟨https://www.jax.org/⟩.

Uchida, Y., Yagi, Y., Takao, M., Takao, M., Tano, M., Umetsu, M., Hirano, S., Usui, T., Tachikawa, M., Terasaki, T., 2020. Comparison of Absolute Protein Abundances of Transporters and Receptors among Blood-Brain Barriers at Different Cerebral Regions and the Blood-Spinal Cord Barrier in Humans and Rats. Mol. Pharm. 17, 2006–2020. https://doi.org/10.1021/acs.molpharmaceut.0c00178.

UniProt [WWW Document], n.d. URL ⟨https://www.uniprot.org/⟩.

Vanlandewijck, M., He, L., Mäe, M.A., Andrae, J., Ando, K., Del Gaudio, F., Nahar, K., Lebouvier, T., Laviña, B., Gouveia, L., Sun, Y., Raschperger, E., Räsänen, M., Zarb, Y., Mochizuki, N., Keller, A., Lendahl, U., Betsholtz, C., 2018. A molecular atlas of cell types and zonation in the brain vasculature. Nature 554, 475–480. https://doi.org/10.1038/nature25739.

Vina-Vilaseca, A., Bender-Sigel, J., Sorkina, T., Closs, E.I., Sorkin, A., 2011. Protein kinase C-dependent ubiquitination and clathrin-mediated endocytosis of the cationic amino acid transporter CAT-1. J. Biol. Chem. 286, 8697–8706. https://doi.org/10.1074/jbc.M110.186858.

Watson, C.P., Pazarentzos, E., Fidanboylu, M., Padilla, B., Brown, R., Thomas, S.A., 2016. The transporter and permeability interactions of asymmetric dimethylarginine (ADMA) and L-arginine with the human blood–brain barrier in vitro. Brain Res 1648, 232–242. https://doi.org/10.1016/j.brainres.2016.07.026.

Weidenfeller, C., Schrot, S., Zozulya, A., Galla, H.J., 2005. Murine brain capillary endothelial cells exhibit improved barrier properties under the influence of hydrocortisone. Brain Res 1053, 162–174. https://doi.org/10.1016/j.brainres.2005.06.049.

Weksler, B., Romero, I.A., Couraud, P.-O., 2013. The hCMEC/D3 cell line as a model of the human blood brain barrier. Fluids Barriers CNS 10, 16. https://doi.org/10.1186/2045-8118-10-16.

Werner, A., Pieh, D., Echchannaoui, H., Rupp, J., Rajalingam, K., Theobald, M., Closs, E. I., Munder, M., 2019. Cationic Amino Acid Transporter-1-Mediated Arginine Uptake Is Essential for Chronic Lymphocytic Leukemia Cell Proliferation and Viability. Front. Oncol. 9, 1–14. https://doi.org/10.3389/fonc.2019.01268.

Wiedmer, T., Ingles-Prieto, A., Goldmann, U., Steppan, C.M., Superti-Furga, G., 2022. Accelerating SLC Transporter Research: Streamlining Knowledge and Validated Tools. Clin. Pharmacol. Ther. 112, 439–442. https://doi.org/10.1002/cpt.2639.

Winkler, E.A., Kim, C.N., Ross, J.M., Garcia, J.H., Gil, E., Oh, I., Chen, L.Q., Wu, D., Catapano, J.S., Raygor, K., Narsinh, K., Kim, H., Weinsheimer, S., Cooke, D.L., Walcott, B.P., Lawton, M.T., Gupta, N., Zlokovic, B.V., Chang, E.F., Abla, A.A., Lim, D.A., Nowakowski, T.J., 2022. A single-cell atlas of the normal and malformed human brain vasculature. Science 375, eabi7377. https://doi.org/10.1126/science.abi7377.

World Health Organization, 2020. Global health estimates: Leading cause of death in 2019. [WWW Document]. URL ⟨https://www.who.int/news-room/fact-sheets/detail/the-top-10-causes-of-death⟩ (accessed 4.1.23).

Worzfeld, T., Schwaninger, M., 2016. Apicobasal polarity of brain endothelial cells. J. Cereb. Blood Flow. Metab. 36, 340–362. https://doi.org/10.1177/0271678×15608644.

Xie, J., Wang, H., 2017. Semaphorin 7A as a potential immune regulator and promising therapeutic target in rheumatoid arthritis. Arthritis Res. Ther. 19, 10. https://doi.org/10.1186/s13075-016-1217-5.

Yamamoro, R., Kawashima, S., 2022. Pharmacological property, mechanism of action and clinical study results of Pabinafusp Alfa (Genetical Recombination) (IZCARGO® I.V. Infusion 10 mg) as the therapeutic for Mucopolysaccharidosis type-II (Hunter syndrome) [WWW Document]. URL ⟨https://pubmed.ncbi.nlm.nih.gov/34980815/⟩ (accessed 4.28.23).

Yang, A.C., Vest, R.T., Kern, F., Lee, D.P., Agam, M., Maat, C.A., Losada, P.M., Chen, M. B., Schaum, N., Khoury, N., Toland, A., Calcuttawala, K., Shin, H., Pálovics, R., Shin, A., Wang, E.Y., Luo, J., Gate, D., Schulz-Schaeffer, W.J., Chu, P., Siegenthaler, J.A., McNerney, M.W., Keller, A., Wyss-Coray, T., 2022. A human brain vascular atlas reveals diverse mediators of Alzheimer's risk. Nature 603, 885–892. https://doi.org/10.1038/s41586-021-04369-3.

Zhang, W., Liu, Q.Y., Haqqani, A.S., Leclerc, S., Liu, Z., Fauteux, F., Baumann, E., Delaney, C.E., Ly, D., Star, A.T., Brunette, E., Sodja, C., Hewitt, M., Sandhu, J.K., Stanimirovic, D.B., 2020. Differential expression of receptors mediating receptor-mediated transcytosis (RMT) in brain microvessels, brain parenchyma and peripheral tissues of the mouse and the human. Fluids Barriers CNS 17, 1–17. https://doi.org/10.1186/s12987-020-00209-0.

Zhang, Y., Sloan, S.A., Clarke, L.E., Caneda, C., Plaza, C.A., Blumenthal, P.D., Vogel, H., Steinberg, G.K., Edwards, M.S.B., Li, G., Duncan, J.A., Cheshier, S.H., Shuer, L.M., Chang, E.F., Grant, G.A., Gephart, M.G.H., Barres, B.A., 2016. Purification and Characterization of Progenitor and Mature Human Astrocytes Reveals Transcriptional and Functional Differences with Mouse. Neuron 89, 37–53. https://doi.org/10.1016/j.neuron.2015.11.013.

Zhao, Y., Zhang, L., Peng, Y., Yue, Q., Hai, L., Guo, L., Wang, Q., Wu, Y., 2018. GLUT 1-mediated venlafaxine-thiamine disulfide system-glucose conjugates with "lock-in" function for central nervous system delivery. Chem. Biol. Drug Des. 91, 707–716. https://doi.org/10.1111/cbdd.13128.

Zlokovic, B.V., 2008. The Blood-Brain Barrier in Health and Chronic Neurodegenerative Disorders. Neuron 57, 178–201. https://doi.org/10.1016/j.neuron.2008.01.003.

Zuchero, Y.J.Y., Chen, X., Bien-Ly, N., Bumbaca, D., Tong, R.K., Gao, X., Zhang, S., Hoyte, K., Luk, W., Huntley, M.A., Phu, L., Tan, C., Kallop, D., Weimer, R.M., Lu, Y., Kirkpatrick, D.S., Ernst, J.A., Chih, B., Dennis, M.S., Watts, R.J., 2016. Discovery of Novel Blood-Brain Barrier Targets to Enhance Brain Uptake of Therapeutic Antibodies. Neuron 89, 70–82. https://doi.org/10.1016/j.neuron.2015.11.024.